Slope-aspect induced climate differences influence how water is exchanged between the land and atmosphere

T. Eren Bilir[1], Inez Fung[1,2], Todd E. Dawson[1,3]

[1]UC Berkeley, Department of Environmental Science, Policy, and Management
[2]UC Berkeley, Department of Earth and Planetary Science
[3]UC Berkeley, Department of Integrative Biology

Key Points:

- Solar radiation differences generate different microclimates across adjacent north- and south-facing slopes in the midlatitudes
- Continuous high frequency measurements document microclimatic differences and covarying tree water use across a hillslope divide over a dry Mediterranean summer
- Transpiration of a single evergreen tree species is higher on the drier sunnier south-facing slope, suggesting different water use and adaptation strategies.

Corresponding author: T. Eren Bilir, `tebilir@berkeley.edu`

Abstract

High resolution air temperature, relative humidity, soil moisture, insolation, and sap velocity observations on 14 madrone trees spanning adjacent north and south slopes at the University of California's Angelo Coast Range Reserve show that cross-slope climate differences in the mid-latitudes are ecologically important, and impact vegetation-mediated water balance between the earth surface and the atmosphere. In this paper, we describe the cross-slope differences in direct observations of vapor pressure deficit (VPD) and sap velocity, which we use as a proxy for transpiration. We use a hybrid observation/model approach to estimate cross-slope insolation variations. We show that trees on opposing slopes do not follow a shared pattern of physiological response to transpiration drivers, meaning that the observed sap velocity differences are not due entirely to observed microclimate differences, but also due to population-level physiological differences, which may indicate acclimation to inhabited microclimate. While our present dataset and analytical tools do not positively identify any mechanism of possible acclimation, we speculate that differing proportions of sun-adapted and shade-adapted leaves, differences in stomatal regulation, and cross-slope root zone moisture differences could explain some of the observed and modeled differences.

Plain Language Summary

The transfer of water from plants to the atmosphere is determined by the interaction between plant physiology and local microclimate. We made high frequency observations of sap velocity in two populations of Pacific madrone trees across a hillslope divide containing a strong microclimatic gradient. The differences in sunlight between the two slopes lead not only to different temperatures and humidities, but also to differences in energy available for photosynthesis, and hence transpiration. As a result, trees on the south-facing slope transpire 20% more water over the dry Mediterranean summer. Furthermore, we found that water use by trees on the north slope bears a different relationship to environmental conditions than water use by trees on the south slope.

1 Introduction

Plant transpiration is a major conduit for the transfer of water from the land to the atmosphere (Jasechko et al., 2013), and our understanding of how complex and sensitive the leaf-to-atmosphere link is to localized feedbacks, such as slope exposure and

associated conditions, is increasing (e.g., P. Link et al. (2014); Harrison et al. (2020); Amitrano et al. (2019)). Slope aspect influences microclimate (ambient air temperature (T), vapor pressure deficit (VPD), soil moisture, and light) directly via insolation differences, and this effect varies depending on latitude and slope characteristics. Cross-slope microclimate differences provide a natural laboratory for investigating the physiological response of vegetation to altered T, VPD, and light regimes, as other environmental factors such as precipitation, underlying lithology and soil type, and cloud cover are comparable between adjacent hillslopes. Investigation of water dynamics in this setting yields insights into how vegetation–atmosphere water cycle interactions may evolve under future climates with different temperature and VPD regimes, which contributes to more accurate projections of anticipated water fluxes under an altered climate.

The influence of natural microclimatic variations that can be associated with topographic position on vegetation water dynamics is poorly understood, and hence often omitted in models, due to a lack of data (Mencuccini et al., 2019). No prior work has, to our knowledge, investigated cross-slope transpiration dynamics in any of North America, nor in a Mediterranean ecosystem, nor with such density of sap velocity observations focused a single species. Prior work which investigated interspecies transpiration differences among five dominant tree species at our site reveals the importance of controlling for species in order to accurately capture the species-specific signatures of transpiration timing and volume, which can be large in this ecosystem: at the extreme, differences in forest composition in the North Coast Range could alter anticipated surface temperatures by up to 3°C during the hottest summer months (P. A. Link, 2015).

We present a set of field observations and modeling exercises designed to investigate the effect of disparate microclimates on water fluxes from a single species of deeply-rooted drought-tolerant broadleaf evergreen tree. We use the climatic gradient created by differences in solar radiation on adjacent north- and south-facing slopes of a hill to explore the impact of variable microclimate on sap velocities, and thus transpiration, in this single species of tree. We define microclimate by ambient air temperature and humidity beneath the canopy, incoming solar radiation adjusted for the slope and aspect of the closed canopy, and soil moisture measured at 30 cm.

In the following sections, we describe the research site and our network of direct observations, including our hybrid observation/model approach to simulating sunlight.

We then give a detailed analysis of the climatic features and sap velocity measurements of the two slopes, and present our parameterization of a transpiration model based on these cross-slope differences in microclimate and sap velocity. We conclude by exploring the implications of cross-slope differences in ecological response parameters for forest resilience in this region under future climates, including a discussion of the limitations of our analysis and proposed next steps.

2 Methods

2.1 Site description

At the University of California's Angelo Coast Range Reserve (39.729167, -123.644444), a site with large variation in year-to-year precipitation (e.g., 1027 mm in 2013-14, 2991 mm in 2016-17), there exists a heavily instrumented site spanning a forested north-facing slope. The forest is composed of mixed broad-leaf and needle-leaf evergreen trees typical of the Douglas fir Pacific alliance (USDA, 2008). Over a 8000 m^2 area, slightly larger than a standard soccer field, over 1000 instruments have been collecting data since 2009. Weather stations, wells, soil moisture probes, sap velocity sensors, streamflow gauging stations, hanging arrays of temperature and humidity sensors, and a deep (25 m) lateral rock moisture sampling apparatus shed light on the path of water through this ecosystem.

For the first time at the site, our installations take the observations to the south slope. Because of the near-direct north–south orientation of the hillslope, the microclimatic differences between the two slopes are pronounced. The north slope of the hill is cool and moist and has a river (Elder Creek) at the bottom. The south slope of the hill is comparatively hot and dry and has no river. Our direct observations show that the south slope can be nearly 7°C hotter and experience VPDs of up to 1.8 kPa greater during late September mornings (see Table 1). There is a visible transition in tree species composition across the ridge of the hill (see Figure 1). Because these are two sides of the same hill, we assume precipitation inputs and cloud-induced variations in solar radiation are identical.

For the purposes of examining cross-slope differences in sap velocity, we focus on the dry months (June–October). This is because the seasonal drought in California's Mediterranean climate simplifies our environmental conditions firstly by avoiding potential post-

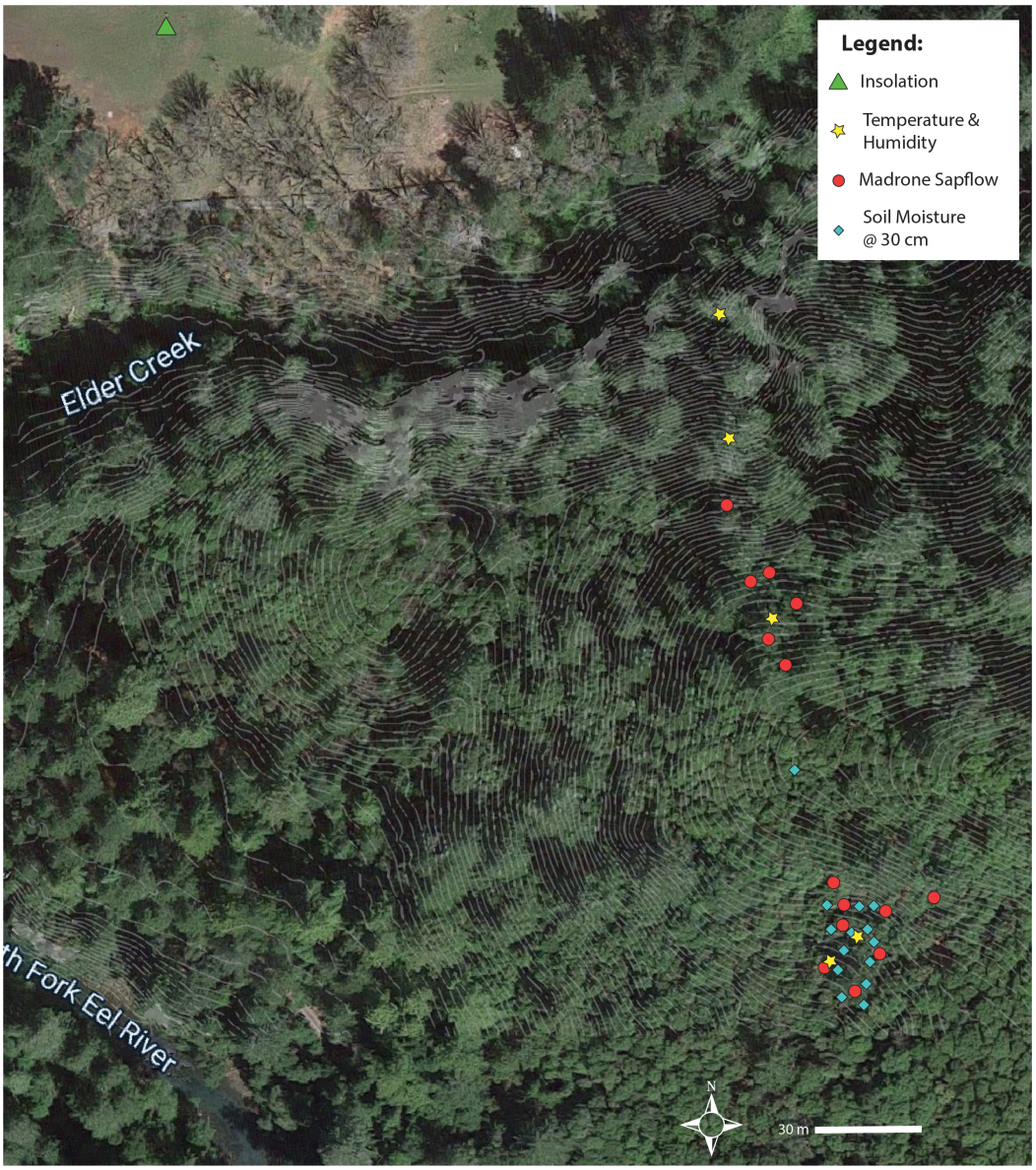

Figure 1. A map of the Rivendell field site in Northern California (39.729167, -123.644444), and the locations of data for this analysis. The canopy covering the north slope is largely made up of Douglas fir (*Pseudotsuga menziesii*), bay (*Umbellularia californica*), and evergreen oak tree species (Tan oak *Notholithocarpus densiflorus*, Coastal live oak *Quercus agrifolia*, Canyon live oak *Quercus chrysolepis*), with some Pacific madrone trees (*Arbutus menziesii*) in the upper half of the hillslope. In contrast, the south slope is mostly populated with Pacific madrone trees, with a few Douglas fir and oak trees primarily occurring in the upper half of the slope near the ridge. 1 m topographic lines are shown in light gray. Underlying high-resolution satellite imagery is from Maxar Technologies, accessed through Google Earth Engine (Gorelick et al., 2017).

rain leaf wetness (leading to possible sunny conditions with low transpiration), and secondly by simplifying the correlation of 30 cm moisture dynamics with those of deeper moisture layers, which the trees at this site are accessing (Oshun et al., 2016). Thirdly, during a time of continuously declining subsurface moisture availability, we hypothesize that above-ground microclimatic variations may have the largest impact.

We focus on Pacific madrone (*Arbutus menziesii*) for two reasons: Firstly, their prevalence on both slopes at our site in particular allows for higher rates of same-species sampling. Secondly, prior work on the north slope at this site (P. Link et al., 2014) has shown that madrone trees reach their peak sap velocities latest in the dry season, around mid- to late-July, compared to other neighboring evergreen species on the site, which reach their peak sap velocities up to two months earlier when soils are wetter. Thus, madrone trees experience their sap velocity peak during the highest VPD conditions in combination with the lowest soil moistures of any other tree species at our site. We hypothesized that this would make madrones trees more sensitive to strong above-ground climate gradients, potentially resulting in a larger cross-slope signal in the sap velocity data.

2.2 Instrumentation

The field study collects 1) sap velocity measurements on Pacific madrone trees; 2) ambient understory temperature and humidity microclimate; 3) incoming solar radiation to an open meadow adjacent to the site; and 4) soil moisture at 30 cm (Figure 1).

Sap velocity sensors (Dynamax Granier-style Thermal Dissipation Probes, as in Granier (1985) and Granier (1987)) are installed into 14 madrone trees, 8 on the south slope and 6 on the north slope (Figure 1, red dots). Each tree has two 80 mm long sensors with thermocouple junctions at 15 and 70 mm, and sensors are placed approximately 180°apart. We consider only data from the outer thermocouple junctions, at 15 mm depth, resulting in 16 and 12 data streams on the south and north slopes, respectively. Sixteen soil moisture sensors (Campbell Scientific CS650) monitor surface soil moisture at 30 cm in a network that covers the south slope and ridge area (Figure 1, blue diamonds). Unfortunately, similar soil moisture observations on the north slope were compromised during the study period, and are therefore not used in this study. Three temperature and humidity sensors (Campbell Scientific CS215) are installed 4-6 ft above the ground in weather stations on the north slope, while eleven exist on the south slope, ten of which

hang in a vertical string from the canopy to the ground, and the last of which is installed 4-6 ft above the ground in a weather station (Figure 1, yellow stars; vertical string represented as one point). A weather station in an adjoining meadow provides information about incoming radiation, wind speeds, and precipitation (Figure 1, green triangle).

There are several unique aspects of this field work: 1) the high resolution of sap velocity measurements (2 sensors per tree and 14 trees); 2) the comprehensiveness of the hydrological measurements, from ambient microclimate, sap velocities, soil moisture and ground water fluctuations; and 3) the high frequency (<15 minutes) of the measurements (Figure 4), a time scale that is commensurate with time steps of ecological processes in state-of-the-art climate models.

2.3 Data processing

All data are collected at 1- to 15-minute intervals, and resampled to 5 minute intervals, with no interpolation. Cleaning and analysis of field data was conducted with Python 3.7.4.

Sap velocity: Granier-type sap velocity probes present challenges to error quantification, especially with regard to sensor calibration (Davis et al., 2012), the choice of constants in Granier's empirically-derived sap velocity formula, which may be species-specific (Sun et al., 2012), and fluctuations in sapwood heat capacity on time scales of days to weeks (Ward et al., 2017). Additionally, asymmetries in tree tissues circumferentially (Oliveras & Llorens, 2001) result in different sap velocities even when measured at a constant depth. Our study trees ranged from 14-28" in diameter, and we used two probes per tree installed 5.5-6.5 ft from the ground, which we infer based on our own prior experiments is insufficient resolution to capture the true scale of radial variation in sap velocity. Yet, because the probes intrude into critical water-transporting tissues, oversaturating a tree with sensors may stress the tree, changing the degree to which the data streams can represent an undisturbed population.

We confront these issues by assuming that any uncertainty introduced by variation in construction or calibration of sensors, or from incomplete sampling of radial sap velocity variation, is randomly distributed in our data set. We also assume that, given our focus on a single tree species, using sap velocity equation constants validated for madrone in specific is unnecessary, as our data all received identical scaling and no cross-species

comparisons are made. Fluctuations in sapwood heat capacity are corrected via the standard practice of continuously redetermining a unique local 'zero flow' over a particular window of time, to ensure comparability of data collected in different seasons during which tree tissues may have had differing water content (Ward et al., 2017).

Our sap flow data processing begins with applying the standard zeroing procedure to each data stream using a 5-day window. We then looked for outliers among the individual sap velocity data streams, defined as having a mean sap velocity that is more than twice the interquartile range away from the mean sap velocity for the group of sensors representing a particular slope. One outlier on the north slope was identified and excluded, and all remaining data streams were averaged together by slope, resulting in a sap velocity time series for an average north slope madrone tree and an average south slope madrone tree. We assume that the number of remaining data streams on each slope (11 data streams for the north slope and 16 for the south slope) is enough to ensure that no systematic error remains from either endogenous sensor error or incompletely-sampled radial variation in sap velocity. We interpret the standard deviation of our average-tree data streams as representing total uncertainty in our measured sap velocity magnitude. This is illustrated in Figure 2.

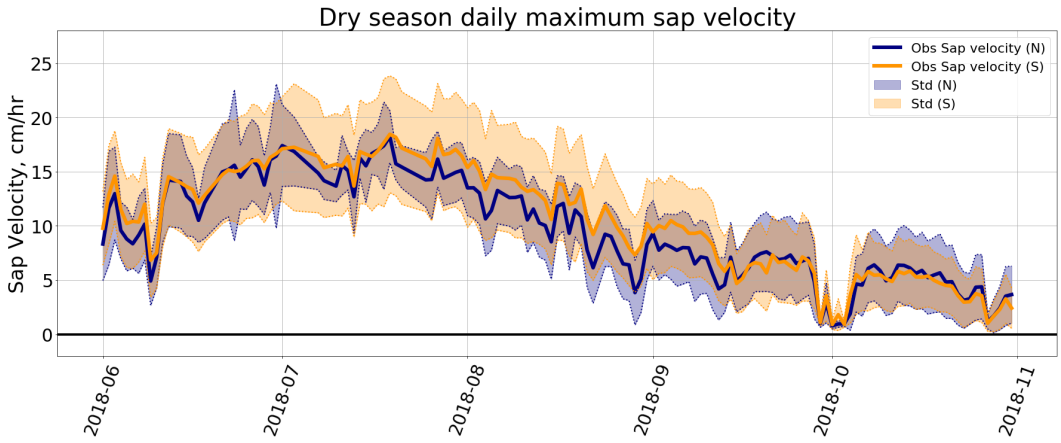

Figure 2. Daily maximum sap velocities for each slope, plotted with +/- 1 standard deviation reflecting spread among the data streams for each slope's tree population. While the south slope has faster peak velocities on average throughout most of the dry season up to the middle of September, during the end of the dry season the north slope experiences faster peak sap velocities on average. Nevertheless, as Figure 6 shows, the south slope transpires more water per sapwood area even during the month of October due to a longer diurnal cycle of transpiration.

VPD: Temperature and humidity are both reported by a single instrument (Campbell Scientific CS215, Figure 1, yellow stars). We averaged temperature and humidity data streams by slope, and then derived vapor pressure deficit (VPD) as:

$$VPD = SVP(1 - RH)$$

where SVP is the saturated vapor pressure (kPa) estimated as a function of temperature by the Clausius-Clapeyron equation (Bolton, 1980), and RH is the directly sensed relative humidity.

Insolation: Unobstructed total (combined direct and diffuse) solar radiation is measured in an adjacent meadow (LI-COR LI200X-L, Figure 1, green triangle). To derive the solar radiation on the north and south slopes, we first derived slope aspect from topographic maps. Because the slope undulates over the area enclosed by observations, we use the average aspect of each sampled tree's location. The south slope's aspect is 189.1°, where 180° is due south; the north slope's aspect is 344.2°, where 360° is due north. Thirdly, we measure the canopy slope from 12 LiDAR cross-sections of the vegetation (e.g. Lee et al. (2016)) on each slope, taken 10 m apart laterally along a N-S axis through the observational footprint. For the north slope, on which broadleaf vegetation makes up a closed canopy understory to a sparse canopy of emergent Douglas fir trees, the slope of the broadleaf vegetation was measured. The south slope's canopy has a slope of 21.97°, while the north slope is steeper, with a broadleaf canopy slope of 32.82°.

The clear-sky direct solar radiation for different times and days (solar zenith and azimuth angles) is calculated using python's 'solarradiation' library (Stafford, 2018) that follows the formulation of Duffie and Beckman (1991). The calculation is done for a flat surface (S_{flat}) as well as for north and south slopes (S_N and S_S, respectively), using the latitude, canopy slope steepness, and slope aspect we have estimated for each slope. To obtain the total insolation for each slope, we scale the total radiation measured at the meadow by the scaling factor for each slope:

$$I_{North} = I_{meadow,Observed} \times \frac{S_N}{S_{flat}}$$
$$I_{South} = I_{meadow,Observed} \times \frac{S_S}{S_{flat}}$$

Figure 3 provides a visualization of the computed solar trajectories for the Riven-dell site and the scaling factors for each slope. The relative angles of the hillslopes and

212 solar trajectories illustrate why it is that early in the dry season, the north slope receives
213 more afternoon sunlight than the south slope, and late in the dry season, the north slope
214 gets very little direct sunlight at all. Late in the dry season, the south slope receives more
215 sunlight than the flat meadow, while the north slope receives less.

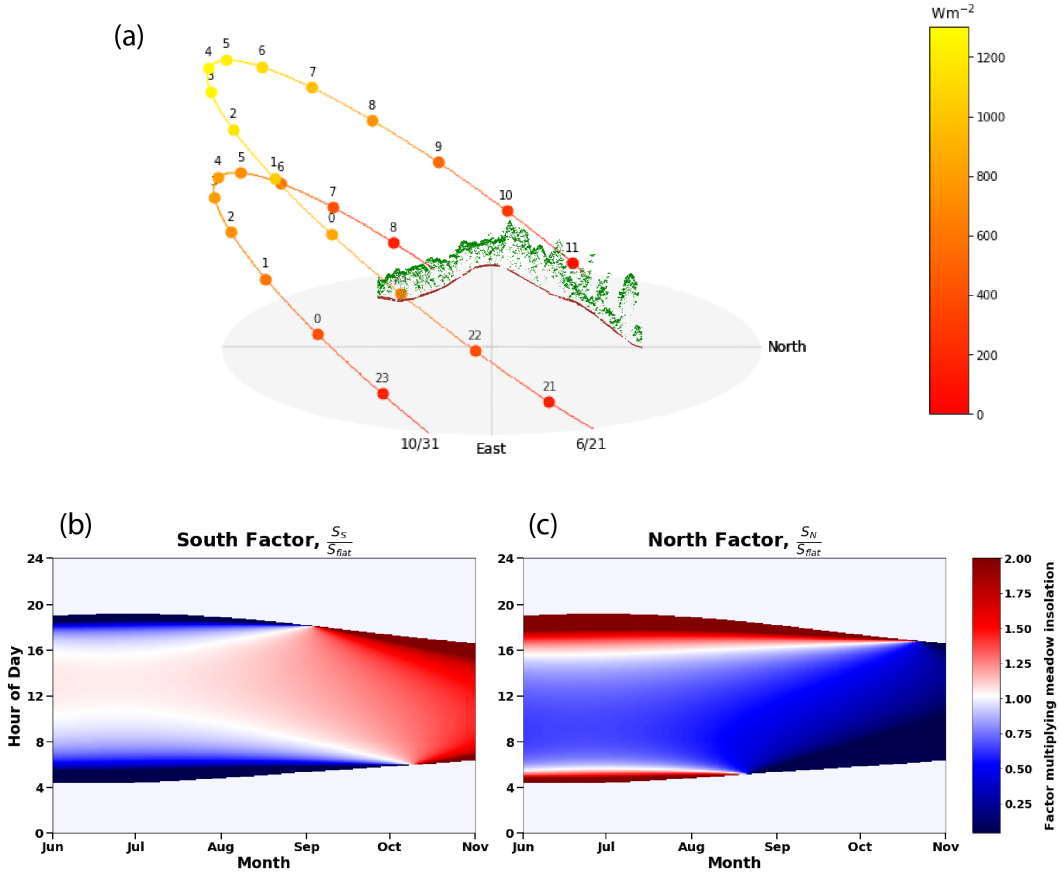

Figure 3. A summary of the solar model. Panel a: The solar trajectories at the latitude of the Rivendell site for the summer solstice (6/21) and the end of the dry season (10/31), showing that the sun rises and sets north of due East and due West for part of the dry season. The numbers indicate local time. A LiDAR cross section of the Rivendell site is provided for orientation. Panels b) and c): the scaling factor for each slope's insolation, as it evolves throughout the day (y-axis) and the dry season (x-axis). The asymmetry in panels b) and c) reflects the slightly westward aspect of both slopes, also visible in Figure 1.

216 **Soil Moisture:** Our dense network of 14 soil moisture sensors at 30 cm (CS650
217 Water Content Reflectometers, Figure 1, blue diamonds) shows large-magnitude vari-

ation in soil volumetric water content at a roughly 15 m length scale, independently confirmed by a limited amount of manual soil sampling. This variation in shallow soil moisture is spatially organized, and appears to relate to the geomorphology and history of shallow landslide disturbance in the area (W. Dietrich, private communication). This variation does not appear to be correlated with variation in sap velocity magnitude of proximate trees, suggesting lateral and vertical extents of the tree roots may be accessing moisture from a wider area and from deep moisture in weathered bedrock (Rempe & Dietrich, 2018; Vrettas & Fung, 2017). Lacking observations to capture these deep moisture reservoirs, we assume that the overall dynamics of root-zone moisture are correlated with those of 30 cm soil moisture over the summer dry season (i.e., both show a steady decline), and use a site-wide average of 30 cm soil moisture for both slopes.

3 Results & Discussion

3.1 Microclimate and sap velocities on the north and south slopes

To illustrate the high-frequency data stream, Figure 4 shows, for the dry season and beginning of the wet season (June–October) of 2018, the average microclimate and sap velocity data for the north and south slopes, as well as the averaged soil moisture data for the south slope. While soil moisture shows a steady decline through the dry summer, sap velocities on both slopes peak in July when 30 cm soil moisture is generally around 10%, about 1-2 months after the start of the dry season.

Monthly climatologies of the diurnally cycling variables (i.e., all except soil moisture) display the microclimate and sap velocity differences between the two slopes, and provide a snapshot of how these variables evolve together throughout the dry season (Figure 5). In the diurnal cycle, both the south and north slopes show sap velocities that peak, not surprisingly, around mid-day. However, the south slope sap velocity is substantially faster than north slope sap velocity in late morning, while the north slope flows slightly faster than the south slope in the late afternoon and early evening. The cross-slope dynamics of the sap velocity diurnal cycles are also descriptive of the cross-slope dynamics of the diurnal cycles in above-ground microclimate.

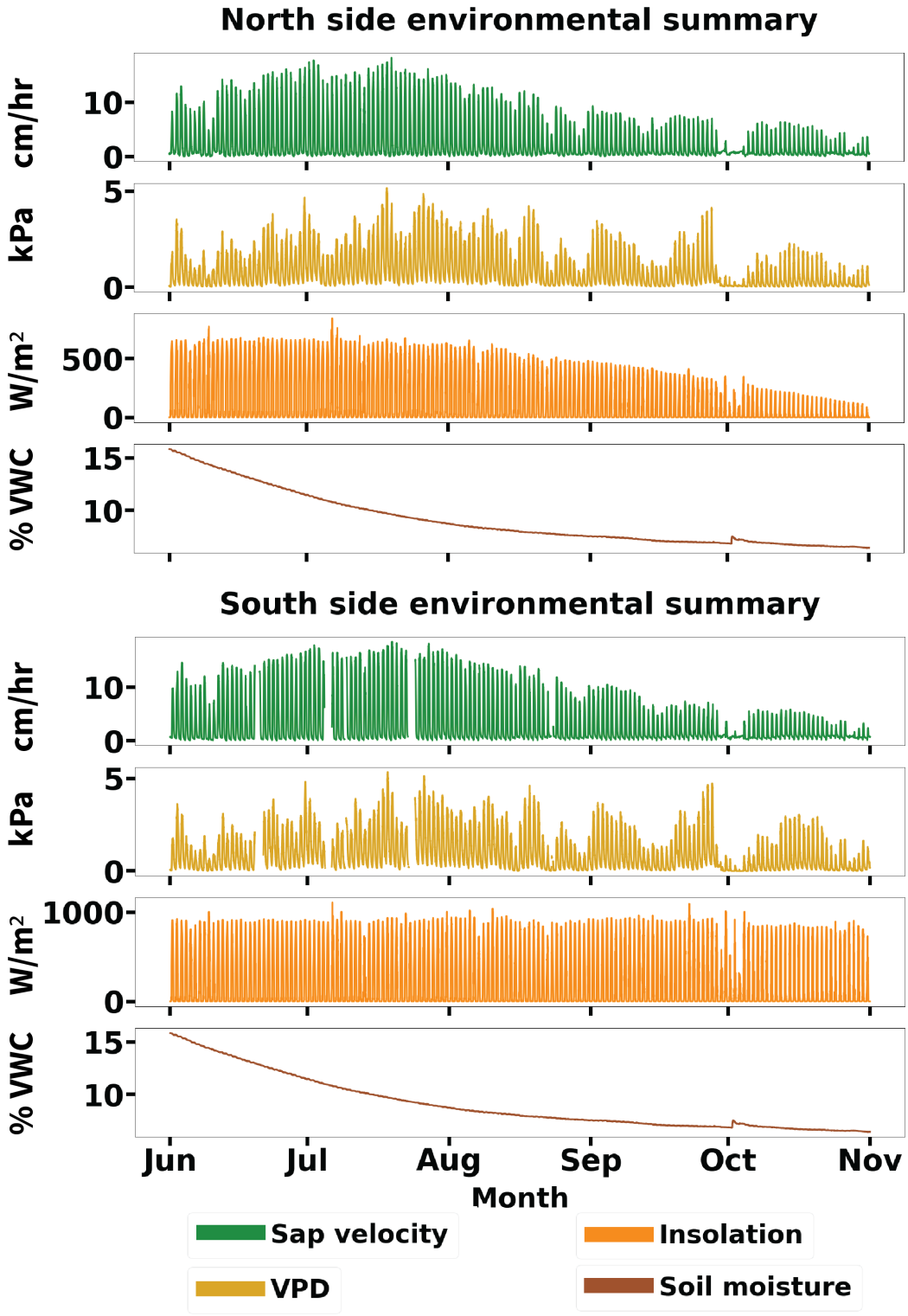

Figure 4. Time series of environmental drivers of sap velocity for each slope, showing what the MCMC parameterization process used as inputs. Soil moisture is identical for both slopes in this set up, though we tested other representations (see Figure 8). Sap velocities decrease to near zero during a rainstorm in early October when both insolation and VPD decline, and soil moisture increases. Thereafter both VPD and sap velocities picked up while soil moisture continues to decline. Day-to-day variations in VPD are large and show no significant trend through the dry season, but insolation varies substantially on the north slope over the dry season.

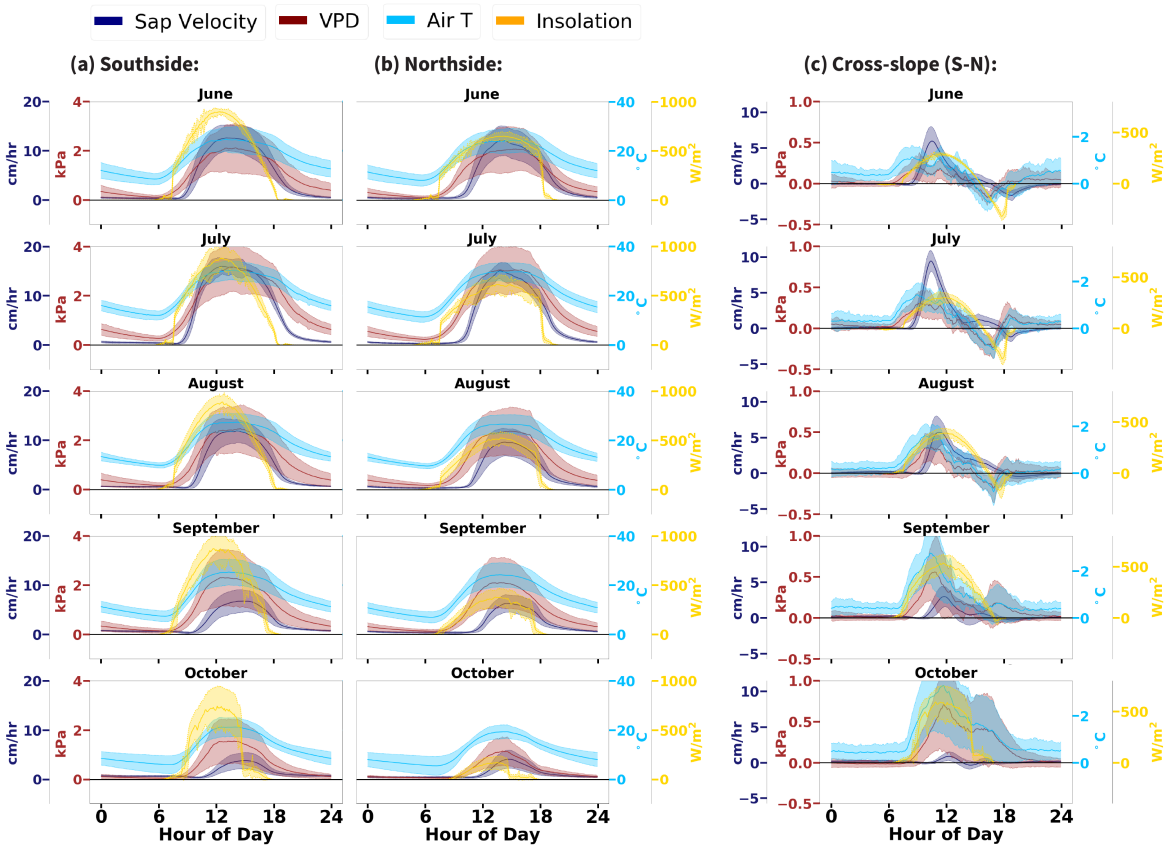

Figure 5. Monthly climatologies of diurnally cycling environmental drivers of sap velocity. Shading shows +/- 1 standard deviation of the monthly climatology, and thus reflects the variability over the month. For all the months of the dry season and on both slopes, while air temperature (pale blue) rises and falls in close concert with the sun (yellow), the VPD diurnal cycle (burgundy) lags behind, and sap velocity (purple) lags behind even further. Though cross slope differences in sap velocity peak in July, the cross-slope microclimate differences peak in the late dry season, in September and October.

Table 1: A month-by-month summary of shifting environmental conditions on each slope. Rows labeled "Max" refer to the maximum value observed over the whole month, and values are reported with the date, hour, and minute recorded. "ClmMax" refers to the climatological maximum, i.e. the maximum of the average diurnal cycle of each variable observed over the whole month. The climatological maxima correspond with the climatologies shown in Figure 5, but the time series maxima show the extremes for the whole month, to help set the context. For instance, in late September and October, the south slope can become nearly 7°C hotter with 1.8 kPa higher VPD, and this climate difference occurs in the late morning-early afternoon. In contrast, in July, the month of peak sap velocity and cross-slope sap velocity differences, the largest cross-slope temperature and VPD differences are less than half the magnitude seen in October.

Sap Velocity (cm/hr) Maxima, by month:					
	June	July	August	September	October
Max (N)	**16.44** 06-30 15:55	**18.22** 07-19 13:55	**13.51** 08-02 13:45	**9.30** 09-01 14:00	**6.40** 10-08 14:25
Max (S)	**16.65** 06-30 15:35	**18.45** 07-19 13:00	**16.01** 08-02 13:40	**10.48** 09-04 14:05	**5.83** 10-14 15:10
Max (S-N)	**9.54** 06-30 10:05	**11.35** 07-25 10:20	**9.16** 08-01 10:50	**5.79** 09-04 11:25	**2.38** 10-04 12:55
Max (N-S)	**3.23** 06-23 18:45	**3.11** 07-01 18:50	**0.94** 08-07 19:45	**2.41** 09-20 14:25	**1.53** 10-19 14:25
ClmMax (N)	**12.08**, 14:15	**15.05**, 13:50	**9.65**, 14:20	**6.30**, 14:25	**4.09**, 14:50
ClmMax (S)	**12.62**, 13:05	**16.00**, 12:35	**11.89**, 14:05	**6.77**, 14:55	**3.83**,15:00
ClmMax (S-N)	**5.97**, 10:30	**9.44**, 10:20	**5.72**, 11:15	**2.99**,11:45	**0.92**,12:15
ClmMax (N-S)	**1.66**,18:45	**1.19**,18:40	**0.46**,19:40	**0.27**,18:40	**0.32**,14:30
VPD (kPa) Maxima, by month:					
Max (N)	**4.66**	**5.13**	**4.21**	**4.13**	**2.27**

	06-30 13:55	07-18 13:55	08-18 14:45	09-27 13:35	10-14 14:25
Max (S)	**4.79** 06-30 13:55	**5.30** 07-18 13:50	**4.59** 08-18 14:35	**4.69** 09-27 12:40	**3.03** 10-16 12:20
Max (S-N)	**0.62** 06-30 20:00	**0.76** 07-17 11:20	**0.88** 08-18 10:55	**1.83** 09-26 10:55	**1.69** 10-13 11:40
Max (N-S)	**0.36** 06-24 16:15	**0.54** 07-28 17:00	**0.46** 08-08 16:55	**0.18** 09-10 17:05	**0.11** 10-27 17:30
ClmMax (N)	**2.07**, 15:25	**3.05**, 16:00	**2.37**, 14:50	**2.09**, 13:50	**1.15**, 14:00
ClmMax (S)	**2.12**, 14:00	**3.16**, 13:20	**2.46**, 14:30	**2.30**, 12:40	**1.56**,13:50
ClmMax (S-N)	**0.20**, 09:10	**0.30**, 09:05	**0.32**, 10:25	**0.56**,10:45	**0.71**,11:45
ClmMax (N-S)	**0.17**, 16:30	**0.23**, 16:50	**0.18**, 16:55	**-0.001**, 06:10	**0.01**, 05:40
Air Temperature (°C) Maxima, by month:					
Max (N)	**34.53** 06-30 14:35	**35.95** 07-18 14:00	**32.21** 08-18 14:50	**32.22** 09-27 14:10	**23.46** 10-13 14:15
Max (S)	**35.20** 06-30 13:55	**36.83** 07-18 13:10	**33.38** 08-18 14:15	**34.34** 09-27 12:35	**27.76** 10-13 13:15
Max (S-N)	**2.54** 06-23 00:25	**2.38** 07-01 08:05	**3.17** 08-18 11:00	**6.34** 09-26 10:55	**6.61** 10-20 11:30
Max (N-S)	**1.97** 06-17 15:50	**1.57** 07-28 17:00	**1.71** 08-21 15:30	**0.89** 09-05 18:25	**0.78** 10-22 17:10
ClmMax (N)	**24.28**, 15:20	**29.67**, 15:50	**26.61**, 14:05	**24.24**, 13:45	**19.37**, 14:25
ClmMax (S)	**24.73**, 12:55	**30.37**, 13:20	**27.34**, 14:15	**25.28**, 13:20	**21.29**,14:15
ClmMax (S-N)	**1.14**, 08:25	**1.44**, 08:55	**1.60**, 09:45	**2.77**,10:20	**3.30**,11:40
ClmMax (N-S)	**0.82**, 16:30	**0.90**, 16:55	**0.79**, 16:55	**−0.30**, 21:20	**−0.41**, 05:10
Insolation (W/m^2) Maxima, by month:					
Max (N)	**774.4** 06-09 16:35	**841.9** 07-06 14:55	**654.5** 08-05 13:50	**475.9** 09-01 13:30	**347.5** 10-04 13:55
Max (S)	**1006** 06-09 11:55	**1108** 07-06 11:55	**1039** 08-10 12:40	**1096** 09-22 12:15	**1006** 10-04 13:55
Max (S-N)	**332.5** 06-09 11:15	**378.9** 07-31 12:15	**479.0** 08-31 11:35	**711.7** 09-30 11:40	**790.9** 10-28 11:45

Max (N-S)	**360.0** 06-20 17:55	**487.8** 07-07 17:50	**277.08** 08-02 17:45	**115.6** 09-01 17:25	**0.00** 10-04 05:55
ClmMax (N)	**650.5**, 14:10	**613.8**, 14:55	**524.4**, 13:50	**380.1**, 13:20	**171.9**, 13:20
ClmMax (S)	**897.5**, 12:25	**883.6**, 12:30	**890.0**, 12:40	**870.0**, 11:40	**743.9**,12:05
ClmMax (S-N)	**288.7**, 11:20	**300.5**, 11:55	**391.0**, 11:45	**534.8**,11:40	**593.2**,10:50
ClmMax (N-S)	**320.0**, 17:45	**298.5**, 17:50	**166.71**, 17:30	**27.5**, 17:15	**0.00**, 05:50

Figure 6 underscores the differences in timing and amount of sap velocity in the diurnal cycle, both for the whole dry season (panel a) and for each month individually (panels b-f). Cumulative integrals of the average sap velocity diurnal cycle show that on average, south slope madrones transpire 20% more water per day over their combined sapwood area during the dry season. August is the month with the peak percent cross-slope difference in sap velocity, with south slope madrones transpiring on average 32% more water per day over their combined sapwood area during this month. While for most of the dry season the average south slope madrone tree moves water as fast or faster than the average north slope madrone tree at their respective moments of daily peak sap velocity, Figure 2 shows that late in the dry season the north slope madrone trees are slightly faster, although they still transpire less per day.

In our data preparation, we eliminated one of the north slope data streams as an outlier. If this outlier is included, the cross-slope differences in integrated sap velocity are ordinally the same for each time period considered, but of much smaller magnitude. For instance, the dry season cross-slope percent difference in integrated sap velocity would be 6.6%, rather than 20.1%, with the outlier included in the north slope average; and August's cross-slope difference would be 13.7% instead of 32.4%. While we believe there are legitimate reasons to exclude this outlier from the set of north slope data streams due to the unique orientation of the canopy of that tree (which faces more westward than northward, decoupling its solar access from the simulated sunlight we use in our analysis), we also believe that the data from the excluded sensor are accurate. This is illustrative of the fact that eleven high-frequency time series of sap velocity on the north slope are inadequate for capturing the full range of possible variation on a steep slope. For this reason, we do not provide a full error analysis for the cross-slope percentage differences

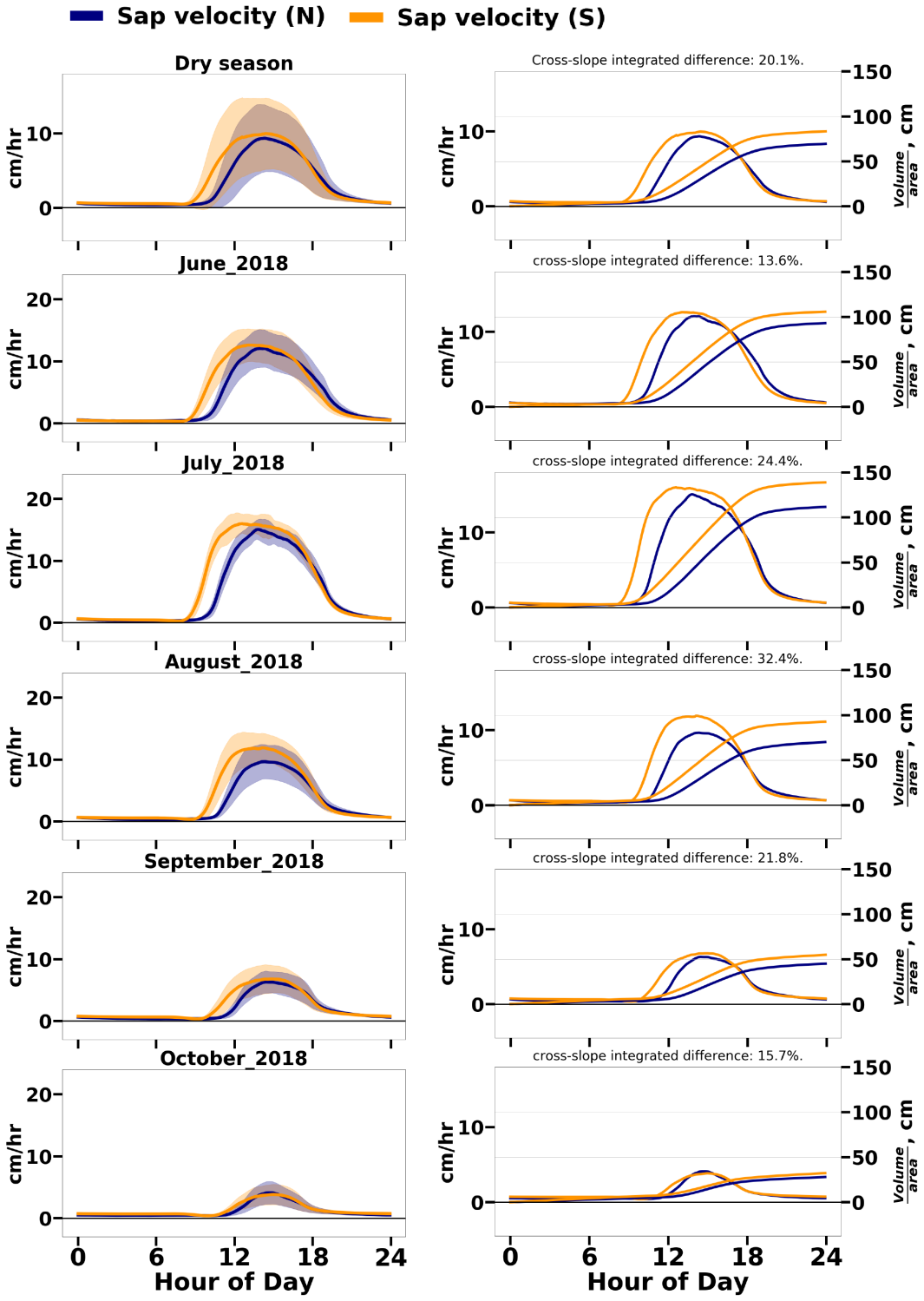

Figure 6. Average diurnal cycles (left panels) and cumulative integrals (right panels) of sap velocity for the entire dry season (June–October, panel a) and by month (panels b-f). The north slope is shown in purple and south slope is shown in orange; shading shows +/- 1 standard deviation of the climatologies, reflecting the variability over the time period (month or dry season). The south slope exhibits higher rates of time-integrated sap velocity, a proxy for transpiration, beginning earlier in the day and also experiencing a longer stretch of high sap velocity. Later in the dry season, the north slope experiences faster peak sap velocities, although it still produces less cumulative transpiration. See Figure 2.

in sap velocity, because more data is required to provide statistically meaningful estimates.

3.2 Description of sap velocity (transpiration) model

To understand the seasonal dynamics of daily maximum sap velocity across different tree species on the north slope of this site, P. Link et al. (2014) apply the conceptual framework of the Jarvis model (Jarvis, 1976) in which the maximum bulk canopy conductance (g_{cmax}) under ideal conditions is modulated by ambient conditions to yield the instantaneous bulk canopy conductance, g_c. Furthermore, by assuming total transpiration E, approximated as $E = g_c \times VPD$, is proportional to the normalized sap velocity v_n with a proportionality constant α: $E = \alpha \times v_n$, they obtain the equation

$$v_n = \frac{g_{cmax}}{\alpha} \times VPD \times f_{VPD}(VPD) \times f_\theta(\theta) * \times f_I(I) \tag{1}$$

The forms of the functions are taken from Lohammar et al. (1980), Feddes et al. (1978), and Waring and Landsberg (2011):

$$f_{VPD}(VPD) = \frac{1}{1 + \frac{VPD}{D_0}}$$

$$f_\theta(\theta) = \frac{1}{1 + exp(-\beta(\theta - \theta_0))}$$
$$f_I(I) = \gamma * (I - 1000) + 1$$

where D_0, β, θ_0 and γ are parameters determined for each tree species using daily maxima of normalized observed sap velocity, VPD, insolation and soil moisture from February 2009 to October 2011.

Equation 1, developed to investigate the seasonality of normalized daily maximum sap velocity across tree species on the same slope (and same microclimate), is not directly applicable for modeling the diurnal cycle during the dry season, where hysteresis in the response of sap velocity to VPD and insolation is observed (Zhang et al., 2014; Gimenez et al., 2019). We modify Equation 1 by allowing for a lag in the sap velocity response to diurnally cycling VPD and insolation of 1 and 2 hours previous. We assume no diurnal variations in soil moisture θ, and thus we do not provide lagged terms for Φ_θ. We

further modified the approach by using averaged, rather than normalized sap velocities, which at substantive n (11 data streams on the north slope and 16 on the south slope) minimizes several potential sources of error that must be considered when using sapflow, and also provides the best match with the scale of our environmental data (see section 2.3). Using averaged rather than normalized sap velocities and splitting the Φ_{VPD} and Φ_I expressions into three led to scaling differences in our parameters compared to P. Link et al. (2014), and in particular, our initial constant, the analog of g_{cmax}/α, has less relation to a theoretical maximum bulk canopy conductance, so for clarity we rename it ε. The resulting model is:

$$
\begin{aligned}
&v_s(t) \\
&\quad = \varepsilon \times \Phi_{VPD}(VPD_t, VPD_{t-1}, VPD_{t-2}) \times \Phi_\theta(\theta_t) \times \Phi_I(I_t, I_{t-1}, I_{t-2}) \\
&= \varepsilon \times \Big(\frac{VPD_t}{1+\frac{VPD_t}{D_0}} \times \frac{VPD_{t-1}}{1+\frac{VPD_{t-1}}{D_{-1}}} \times \frac{VPD_{t-2}}{1+\frac{VPD_{t-2}}{D_{-2}}}\Big) \times \Big(\frac{1}{1+exp(-\beta(\theta-\theta_0))}\Big) \times \\
&\qquad \Big((\gamma_0(I_t-1000)+1) \times (\gamma_{-1}(I_{t-1}-1000)+1) \times (\gamma_{-2}(I_{t-2}-1000)+1)\Big) \quad (2)
\end{aligned}
$$

where t is time, t_{-1} and t_{-2} denote 1 and 2 hours previous, respectively. This results in additional parameters in Equation 2, D_0, D_{-1}, D_{-2}, γ_0, γ_{-1}, and γ_{-2}, in addition to β and θ_0.

3.3 Slope-specific Parameters

To estimate the parameters in Equation 2 for the north and south slopes, we randomly selected 20% of the data (non-sequentially) and assigned it to a training data set, while reserving the remainder for testing. We used Hamiltonian Monte Carlo (Betancourt, 2017), a type of Markov Chain Monte Carlo, and the No-U-Turn Sampler (Hoffman & Gelman, 2014) to derive our parameters for each slope. Parameter estimation used the pymc3 package in python (Salvatier et al., 2016). We repeated this procedure 5 times, to ensure that our parameter estimates did not change substantively depending on the sample assigned to the training data set. Our final reported parameters are the mean of all five runs for each slope. Figure 7 shows the mean parameters as well as the spread of parameters from each of the five runs.

We use the same priors (bounded normal distributions bound at zero; see Table 2) for each model run, to ensure that emergent parameter differences arise from relations in the data and are not forced from priors. Choice of priors is informed through a combination of literature sources and empirical exploration of the data. The priors for the γ parameters are chosen so that the function Φ_I ranges roughly between 0 and 1 over the range of observed insolation. The prior for β is the most restrictive, and is chosen such that both slopes will fit into a tightly curved sigmoid. The south slope data set predictably fits a tightly curved sigmoid even with an uninformative prior, but the north slope data set, appearing to be unconstrained by soil moisture, has the tendency to degenerate into a flat line (i.e., small β, arbitrary θ_0) if not constrained by the prior. The prior for θ_0 is chosen based on an empirically-informed guess at the critical soil moisture threshold that begins to constrain sap velocities. The priors for the D parameters are chosen such that Φ_{VPD} ranges roughly between 0 and VPD_{max}. The prior for ε is chosen to be of the correct magnitude to scale the other portions of the equation to a hypothetical maximum sap velocity. Table 2 shows the means and standard deviations of priors and posteriors for each parameter. The distributions of the parameters estimated for the north and south slopes, and their impact on sap velocities, are shown in Figures 7 and 9.

Table 2: Priors for our MCMC parameterization, and the resulting posteriors. All runs began with identical priors. Posterior means and standard deviations are derived from five separate runs, each using a randomly selected 20% of datapoints.

MCMC parameters				
	Prior mean	Prior SD	Posterior mean	Posterior SD
South Slope Parameters:				
ε	6	60	900	26.0
D_0	3.0	1.0	0.380	1.88 E−2
D_{-1}	3.0	1.0	0.330	1.92 E−2
D_{-2}	3.0	1.0	0.223	9.61 E−3
β	160	6	163	2.32
θ_0	0.07	0.01	7.28 E−2	8.59 E−5
γ	6.0 E−4	2.0 E−4	6.83 E−7	6.81 E−7

γ_{-1}	6.0 E−4	2.0 E−4	8.30 E−4	2.89 E−6
γ_{-2}	6.0 E−4	2.0 E−4	1.20 E−6	1.20 E−6
North Slope Parameters:				
ε	6	60	779	30.5
D_0	3.0	1.0	0.216	1.42 E−2
D_{-1}	3.0	1.0	0.344	2.43 E−2
D_{-2}	3.0	1.0	0.801	3.02 E−2
β	160	8	163	5.94
θ_0	0.07	0.01	3.08 E−2	3.99 E−3
γ	6.0 E−4	2.0 E−4	4.30E−4	1.00E−5
γ_{-1}	6.0 E−4	2.0 E−4	6.08 E−4	1.43 E−5
γ_{-2}	6.0 E−4	2.0 E−4	5.05 E−4	1.76 E−5
Example Soil Moisture Experiment North Slope Parameters: Uniform +2%, Non-linear +5%				
ε	6	60	780	30.4
D_0	3.0	1.0	0.215	1.41 E−2
D_{-1}	3.0	1.0	0.344	2.42 E−2
D_{-2}	3.0	1.0	0.800	3.02 E−2
β	160	6	160	5.98
θ_0	0.07	0.01	6.94 E−2	9.62 E−3
γ	6.0 E−4	2.0 E−4	4.30E−4	1.00E−5
γ_{-1}	6.0 E−4	2.0 E−4	6.08 E−4	1.44 E−5
γ_{-2}	6.0 E−4	2.0 E−4	5.07 E−4	1.76 E−5

The resulting parameterizations for each slope show key differences in response to environmental drivers. With the VPD parameters D_0, D_{-1} and D_{-2}, a larger parameter value points to a greater sap velocity sensitivity to the variable (cf Equation 2). The south slope has D_0, D_{-1} and D_{-2} values of 0.380, 0.330, 0.223, respectively, suggesting that south slope sap velocities are most sensitive to instantaneous VPD, but also to VPD from 2 hours prior, though lagged VPD plays a slightly smaller role. The corresponding values for the north slope are 0.216, 0.344 and 0.801, suggesting that on the north slope VPD_{t-2} has the largest influence on sap velocities.

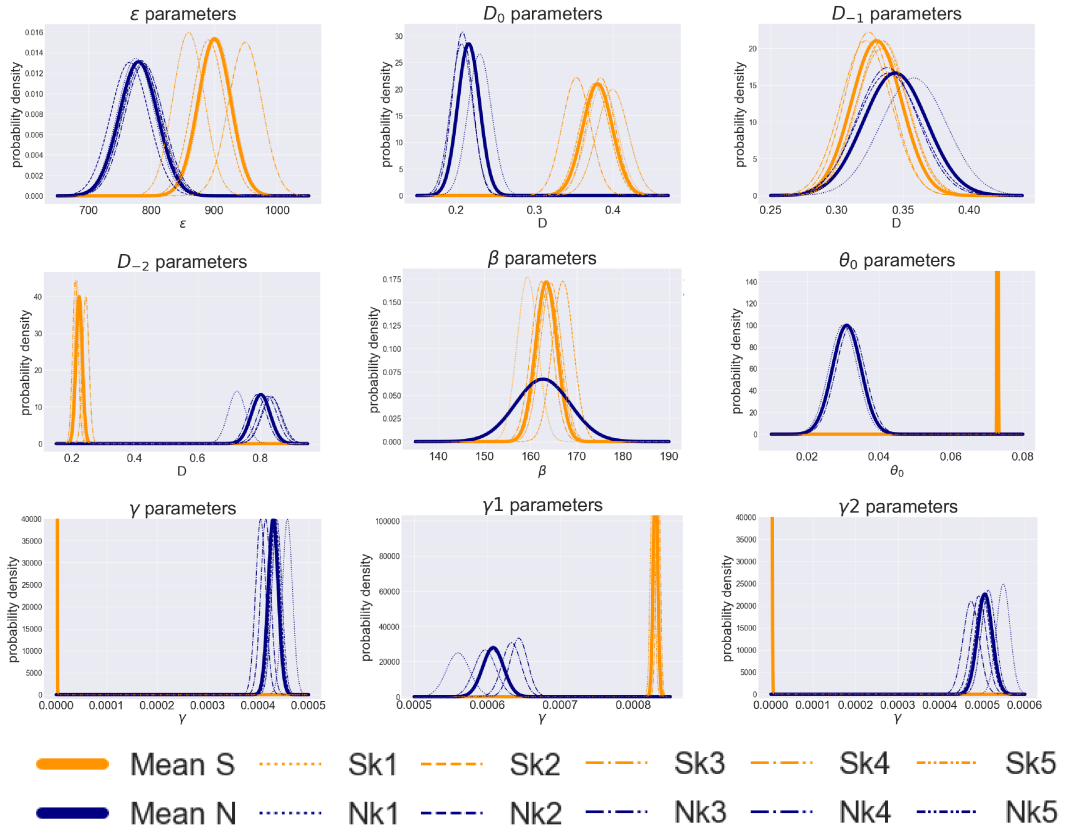

Figure 7. Posterior distributions of fitted model parameters for the north slope (orange) and south slope (blue). Results from each of the five randomly-selected training datasets are shown as dotted lines; and the mean as a bold line. Different subsets of data (k1-k5) used to parameterize the model result in very little difference in the fitted parameters, which is demonstrated in the narrow spread among the thin dotted lines.

The posterior estimates for all D parameters deviate from our prior D by roughly a factor of ten. This is compensated by the growth of ε away from our prior guess. Because Φ_θ and Φ_I vary between 0 and 1, the scaling of modeled sap velocity depends on the product of Φ_{VPD} and ε, which is responsible for the inverse relation in their respective deviations from our priors. Because smaller D parameters change the shape of Φ_{VPD} to a more curved shape, bending the function downward away from the $y = x$ line, and decreases the magnitude of the function overall, this relocation of modeled sap velocity magnitude away from Φ_{VPD} to ε implies that the effect of VPD on sap velocities seen in our observations is less linear, and "saturates" more quickly, than our prior parameters allow. Based on the performance of the resulting models, we interpret that our priors were broad enough to avoid unduly influencing the parameterization process, despite the strong deviation from prior to posterior.

For insolation, the γ_0 and γ_{-2} for the south slope are near zero, suggesting that sap velocities there respond mainly to insolation of the past hour (I_{t-1}). For the north slope, the results suggest that sap velocities are sensitive to contemporaneous insolation as well as insolation of the past two hours, as γ_0, γ_{-1} and γ_{-2} have comparable values.

For soil moisture, β controls the slope of the sigmoid, and θ_0 controls the midpoint. β is similar between the two slopes, while θ_0 differs. The partial function Φ_θ (Figure 9 panel b) shows that while soil moisture is a strongly limiting factor on south slope sap velocities after approximately 10% VWC, it does not cause any limitation for north slope sap velocities. Because soil moisture creates no constraint on sap velocities in the north slope model, there is less certainty in the exact parameter values, as seen in the larger spread of the north slope parameters compared to the south slope parameters (Figure 7).

The lack of soil moisture observations on the north slope leaves uncertainty in the north slope sap velocity response to soil moisture. Our field experience suggests that north slope soils are less dry than the south slope, and while soil moisture is expected to decline through the dry summer, we do not have observations of its magnitude and rate of decline on the north slope. Therefore, we conducted several modeling experiments in which we artificially increased the soil moisture data stream used for the north slope parameterization in both uniform and non-uniform ways: 1) Uniform +5%: we added a uniform 5% increase to observed south-slope soil moisture; 2) Non-linear +5%: we adjusted

the rate of soil moisture decline to half of the observed rate, which amounted to a +5% difference in soil moisture by the end of the dry season; 3) Non-linear +7%: we adjusted the rate of soil moisture decline to one third of the observed rate, which amounted to a +7% difference in soil moisture by the end of the dry season; and lastly, 4) Uniform +2% and non-linear +5%: we added a uniform 2% increase to observed soil moisture, and then additionally adjusted the rate of soil moisture decline to half of the observed rate, which amounted to a +7% difference in soil moisture by the end of the dry season. We then re-ran the north slope MCMC parameterization process with these alternative soil moisture states. We found that between the standard and experimental runs, none of the final parameters changed substantively except θ_0 (Table 2). The changes in θ_0, in light of the co-occuring shift in hypothetical minimum soil moisture, do not undermine the finding that soil moisture is not a limiting factor on the north slope. Put another way, changes to the representation of north slope soil moisture do not appreciably change the shape of Φ_θ, but only shift it along the x-axis with changes in θ_0 (see Figure 8). Thus, we conclude that, in our model, the sap velocities of the north slope are not constrained by soil moisture, and that this conclusion is not rooted in an imperfect soil moisture representation.

To compare the sensitivities of sap velocities on the two slopes to VPD and insolation, we computed mean diurnal cycles of VPD and insolation for July, and use the same mean cycles as inputs to Φ_{VPD} and Φ_I for each slope (cf Equation 2). Figure 9 shows the hysteresis loops in the sap velocity responses. For the same VPD diurnal cycle, the north slope model's Φ_{VPD} attributes more sap velocity amplitude variations to variations in VPD than does the north slope model. This is visible in the greater functional range (plotted on the y-axis) of Φ_{VPD} over the same VPD range (x-axis). Also, at every value of VPD, the north slope model has a larger sap velocity response than the south slope model. This shows that the north slope model has both a higher baseline response to VPD as well as a higher proportional response to increases in VPD than the south slope model. The Φ_I functions show similar responsiveness to sunlight between the slopes, visible in the comparable functional range (y-axis) covered by Φ_I to the same insolation cycle. However, the south slope Φ_I has higher values over the range of observed sunlight. This implies that modeled sap velocity on the south slope has a higher baseline response to sunlight, although the two slopes show proportionally similar responses to increases in sunlight. Lastly, the south slope's soil moisture function shows that the south slope

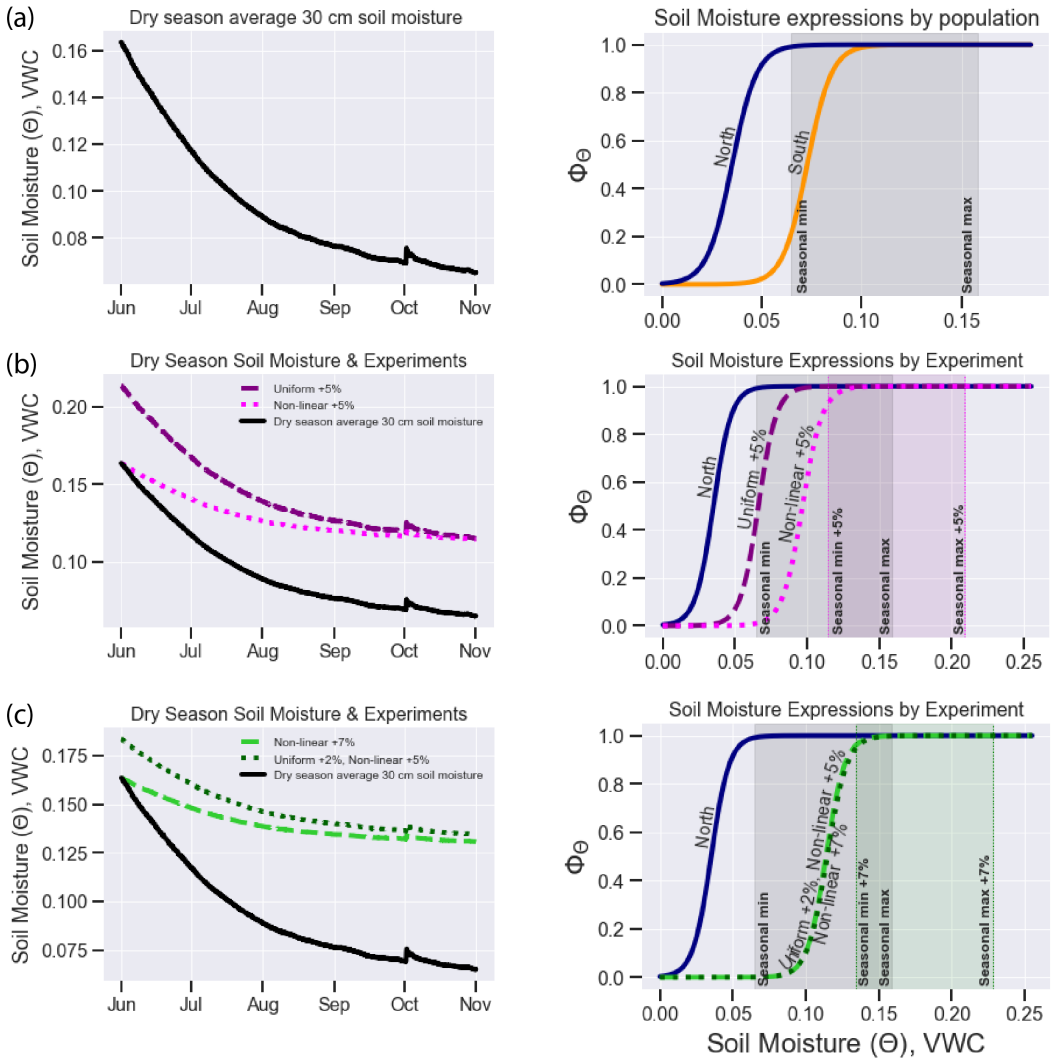

Figure 8. Experimental manipulations of north slope soil moisture time series reveal that under a range of hypothetical conditions, the MCMC parameters fitted for the north slope consistently indicate a lack of soil moisture constraint.

model uses soil moisture as a limiting factor on sap velocity while the north slope model does not, within the range of observed soil moisture over the whole season. Taken together, the model results indicate population-level differences in response to environmental drivers of transpiration. This is explored further in section 3.6.

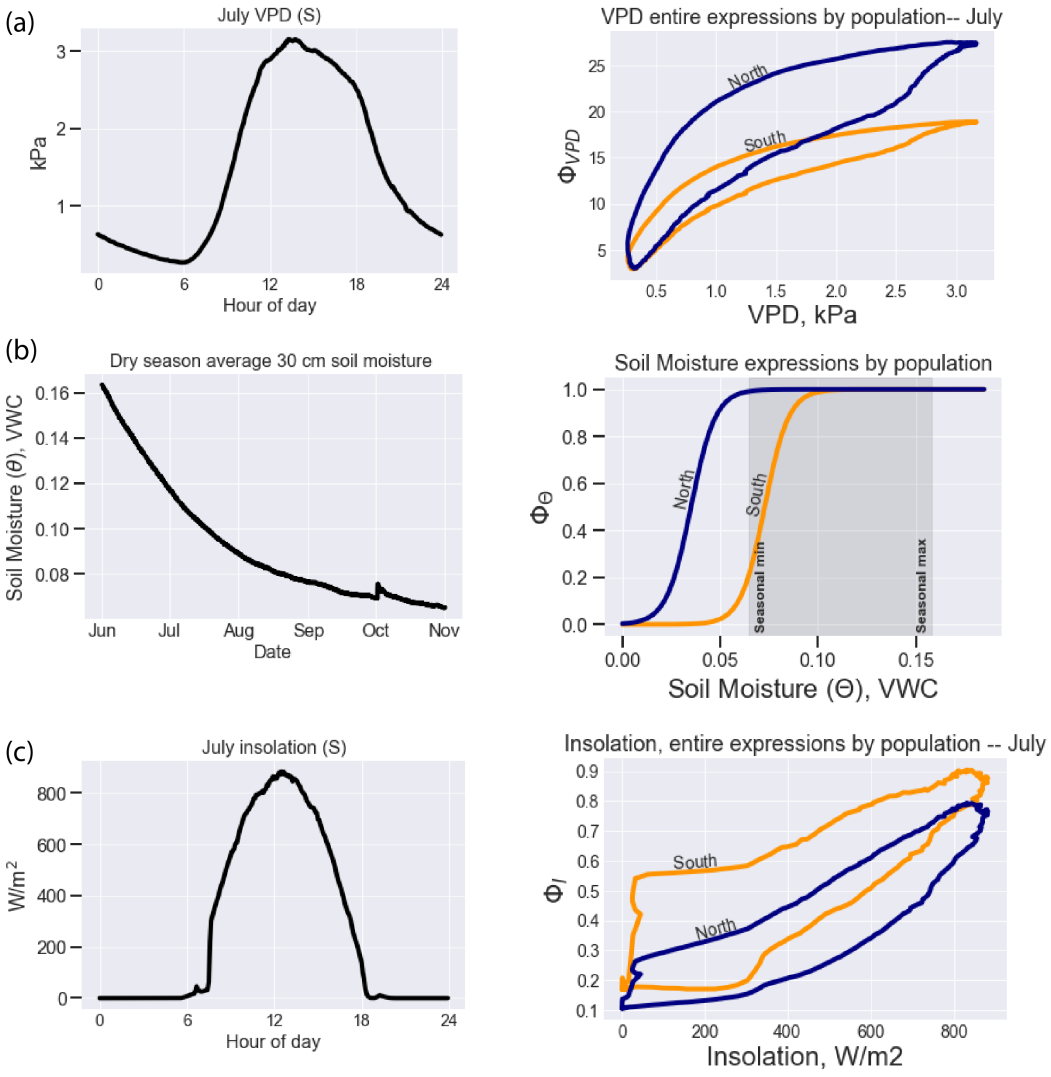

Figure 9. Partial expression plots of Equation 2 show differing sensitivity to environmental drivers among the two populations. The north slope model is more sensitive to VPD, and less sensitive to soil moisture and insolation, indicating that the trees on the north slope do not feel additional transpiration constraint from drying soils over the course of the dry season, beyond that imposed by the light limitation.

Because in our data preparation we excluded an outlier that substantially changed the magnitude of the mean north slope sap velocity, we explored the impact of this outlier by repeating our MCMC analyses with the outlier included. Doing so led to some slight changes in magnitude, but no ordinal differences, in the parameter differences found. The largest differences were in Φ_{VPD}, with the outlier-inclusive average north slope sap velocity even more responsive to VPD, but the conclusions regarding cross-slope differences in parameters are identical both with and without the outlier.

3.4 Model performance

With slope-specific parameters in combination with slope-specific microclimate data streams, we computed model sap velocity data streams for north and south slopes. To assess the performance of our models, we looked at four metrics: a) reproduction of the dry season time series; b) reproduction of dry season time-integrated sap velocity; c) reproduction of dry season climatological sap velocity; and d) reproduction of dry season climatological cross-slope differences in time-integrated sap velocities.

Each set of parameters was applied to its unique test data set, resulting in five similar but separate estimates of the sap velocity time series. These estimates were then averaged together to create our final modeled time series, which was the basis for the nRMSE computed in the test of time series data reproduction (a, Figure 10) and the reproduction of time-integrated sap velocity (b, Figure 11). We also derived average parameter means and standard deviations, which are reported in table 2 and were implemented in our model runs which created our reproduction of dry season climatologies (c, Figure 12) and cross-slope differences in time-integrated sap velocity (d, Figure 12). We opted for presenting our results this way to adhere as closely as possible to the philosophy of keeping our model tests free of any data that was used to derive parameters.

3.5 Influence of parameters vs microclimate

At the heart of our analysis is the question of whether cross-slope differences in sap velocity are proportional to the cross-slope differences in microclimate, or whether population-level differences in physiological function are also playing a role. Our parameter differences indicate population-level differences in physiological function, but as a way of more intuitively visualizing the impact of parameter differences outside the influence of dis-

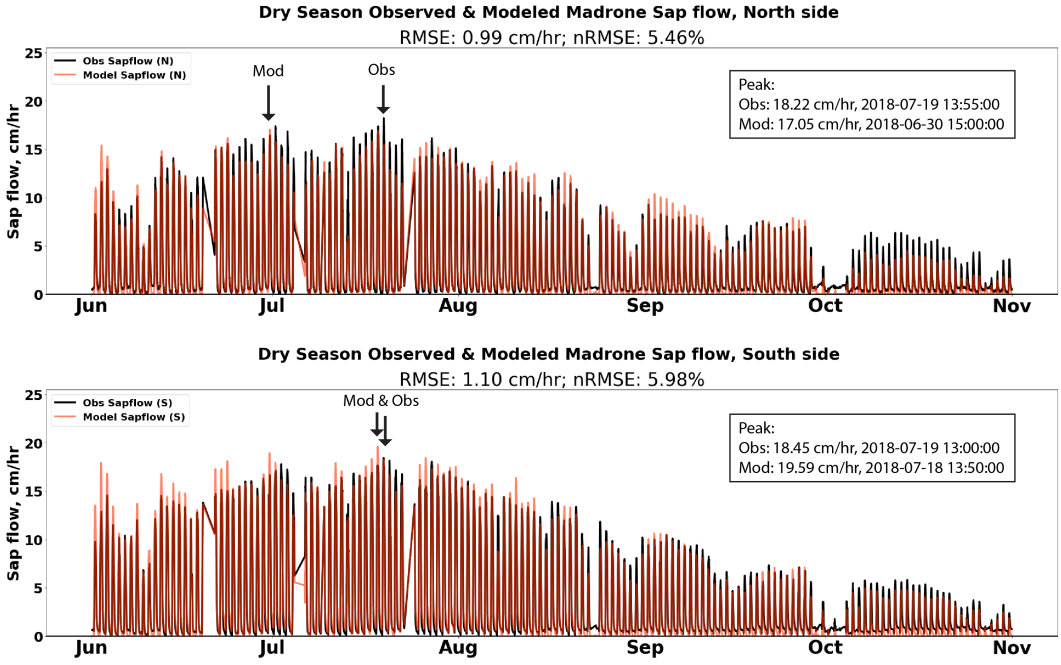

Figure 10. Performance assessment of the model reproduction of the dry season time series. Modeled sap velocity is in red, observations are in black. Model performance measured by nRMSE is similar for both slopes. The south slope model additionally comes close to accurately capturing the time period of seasonal peak sap velocity, while the north slope model is off by nearly a month. However, the month of October stands out as a period where the models systematically underestimate observations for both slopes. We consider reasons for this underestimation in section 3.7.

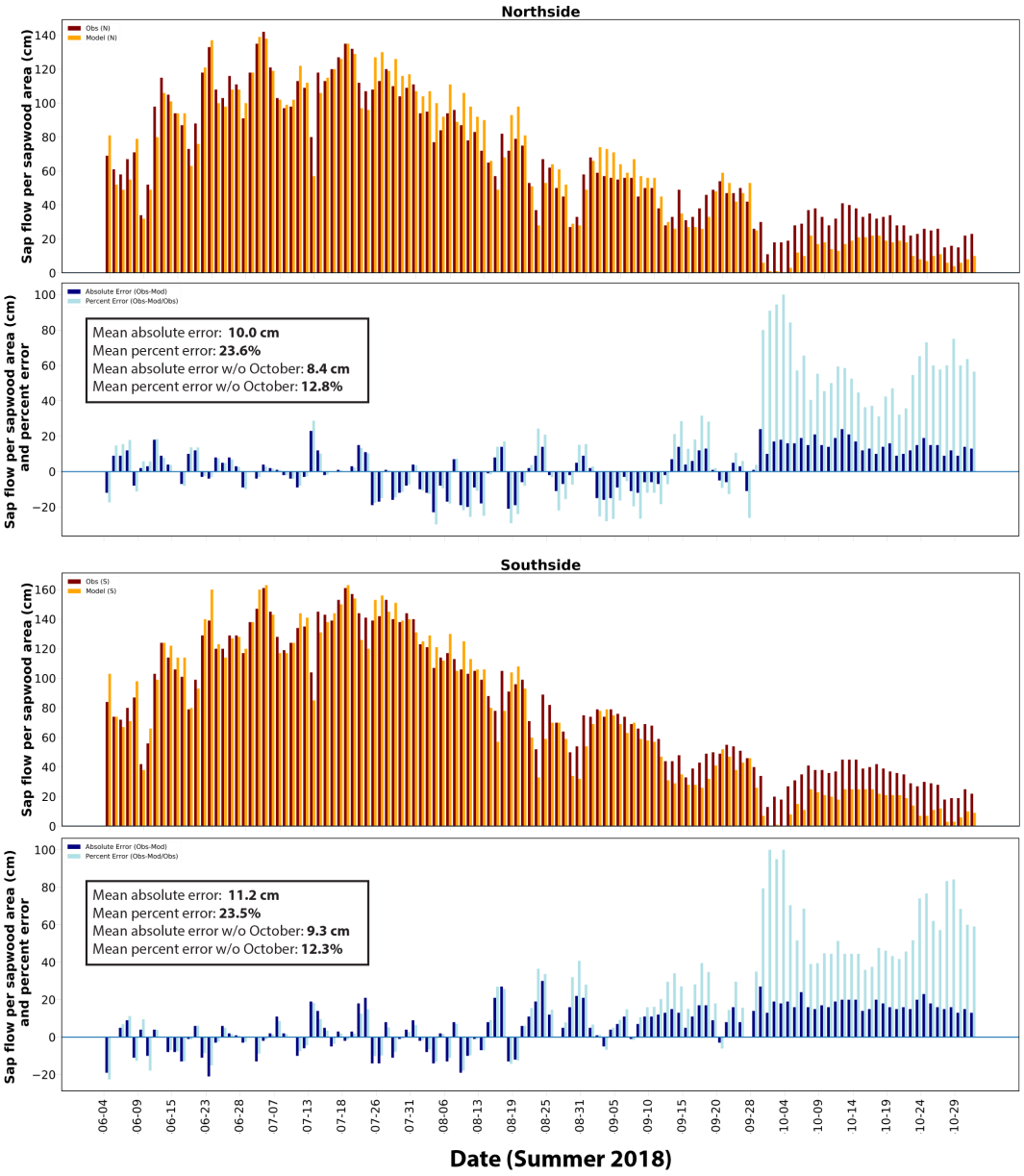

Figure 11. Daily integrals of modeled and observed sap velocities for each slope. The month of October is greatly underestimated due to seasonal shading of the light sensor positioned in the meadow, which is not representative of the tree environment. For the north slope, the model is able to capture 76% of dry season integrated sap velocity, and 87% of June–September integrated sap velocity. For the south slope, the performance is similar, with 76% of dry season integrated sap velocity and 88% of June–September integrated sap velocity represented.

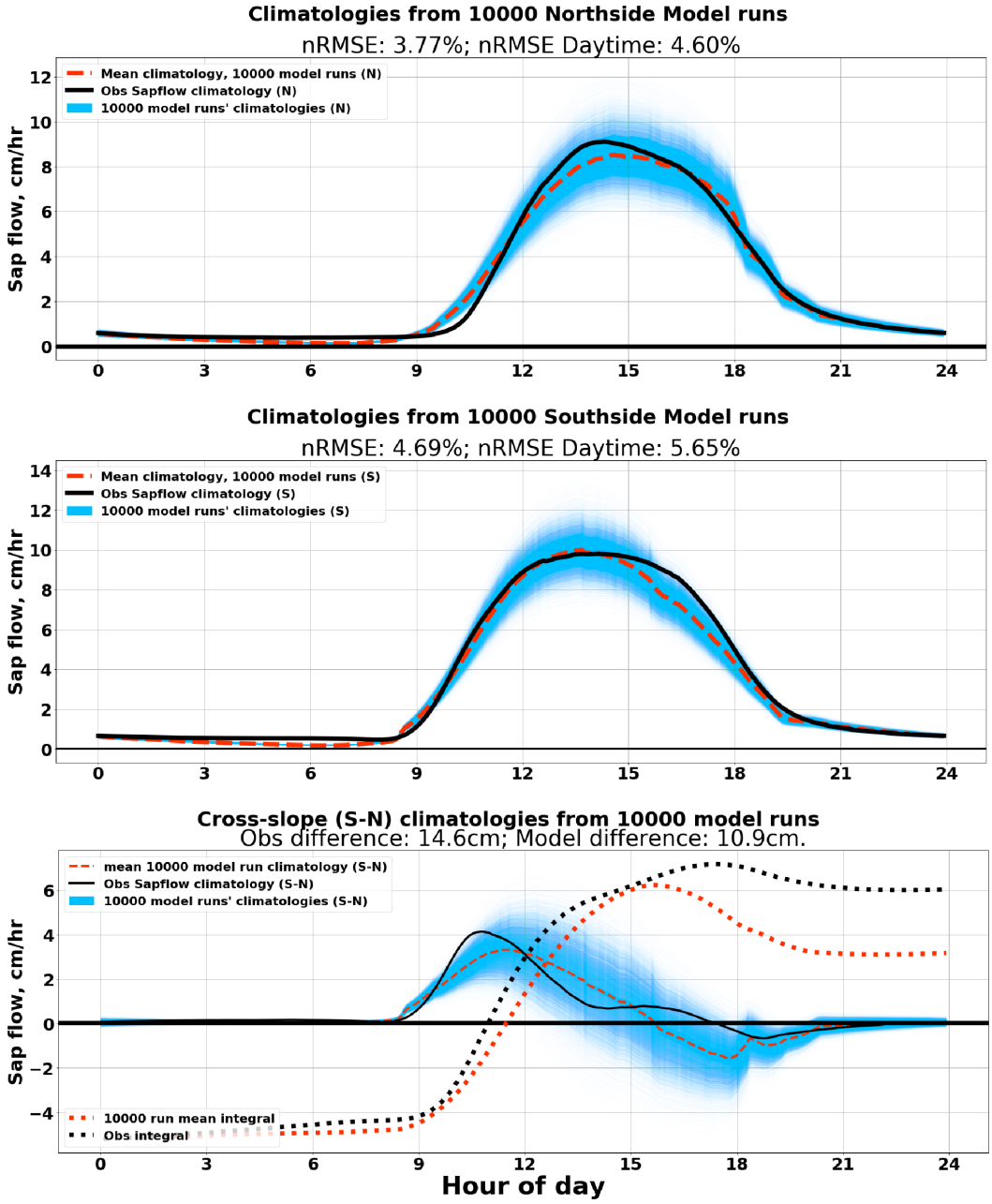

Figure 12. Performance assessment of models relative to the dry season average diurnal cycle. Dry season climatologies of 10,000 model runs are in pale blue, with the mean in red, and observed sap velocity in black. The spread among the 10,000 model runs is a visual indication of model uncertainty arising from spread in the parameter estimates. The normalized root mean square error (nRMSE) of the model comparison to observations is computed relative to the mean of the model runs, and is roughly 4% and 5% for the north and south slopes respectively (top two panels); if error is computed only over the active portion of the diurnal cycle (7am-10pm), this rises to 5% and 6% nRMSE for the north and south models respectively. The models are able to capture 75% of the observed difference in time-integrated sap velocity between the slopes (bottom panel).

parate microclimates, we put our model through a series of simple experiments in which we exchange some or all of the experienced microclimate between the slopes, and observe the response.

We see that the parameter differences lead to dissimilar responses when the models are placed in the same microclimate. The north slope model substantially over-estimates observed sap velocity in the south slope microclimate (Figure 13 panel a), and the south slope model underestimates sap velocity in the north slope microclimate (Figure 13 panel b). Figure 13 (bottom four panels) further shows that while exchanging VPD environment makes very little difference (Figure 13 panel c and d), exchanging the solar radiation environment makes a large difference (Figure 13 panel e and f), and artificially increasing soil moisture increases the sap velocities on the south slope but not the north slope (Figure 13 panel g and h).

The individual responses to environmental drivers, Φ_{VPD},Φ_{θ}, and Φ_{I} (Figure 9) show that the over-estimation of the north slope model in the south slope microclimate is actually not associated with a stronger response to light from north slope trees, but instead with firstly a lack of moisture limitation on sap velocities, and secondly with a stronger response to VPD. Once the north slope model is freed from its light-limited environment by using south slope insolation, the added vigor of its VPD response compared to the south slope model becomes clear.

3.6 Interpretation of sap velocity model results

The divergent parameterizations indicate different physiological responses to environment between the two slopes, after controlling for inhabited microclimate. While none of the parameters in our model is a direct metric of a particular physiological property of the trees, we consider them to represent an aggregation of functional or "behavioral" differences, integrated across all mechanisms that influence sap velocity response to ambient environment, as in the interpretation of the formulas in Jarvis (1976) and Lohammar et al. (1980). We acknowledge that extrapolations of disparate physiological properties between the two tree populations from the differences in the models' statistically-indicated controls on sap velocity can only be speculative, but we explore these speculations to begin a discussion about the degree and kind of acclimation that may exist between trees

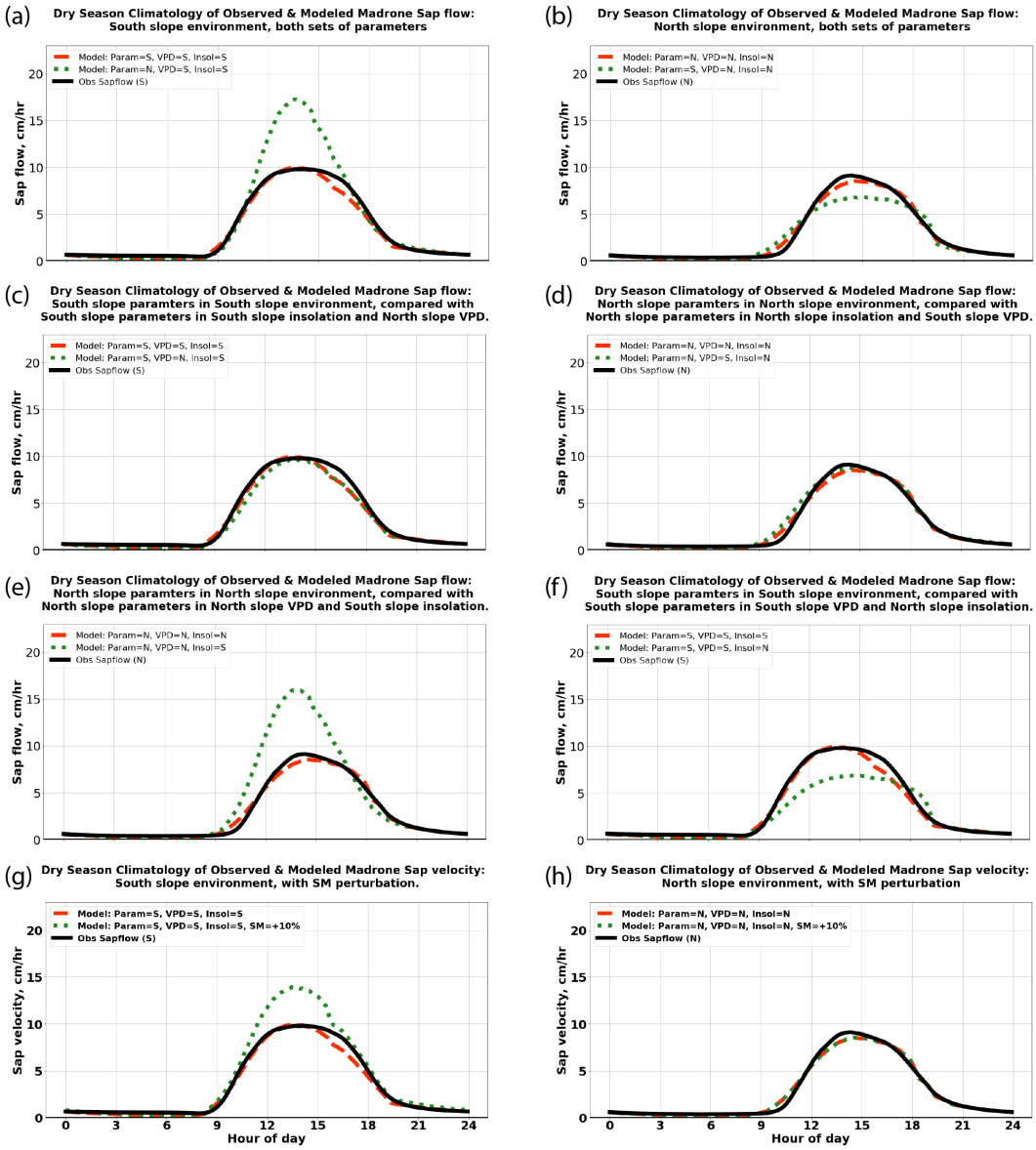

Figure 13. Using the slope-specific models in the opposite slope's microclimate shows the differences in response generated by the two parameterizations to the same microclimate. Panels (a) and (b) show that the north slope model in a south slope microclimate has a more vigorous response than both the south slope model and the observations in the same microclimate, while conversely the south slope model underestimates both the north slope model and observations in the north slope microclimate. Panels (c) and (d) show that while exchanging only the VPD portion of the microclimate between the two slopes makes very little difference to the sap velocities estimated by each model, exchanging the solar radiation environment (panels (e) and (f)) makes a large difference. Panels (g) and (h) show that increased soil moisture increases sap velocities in the south slope model, but not in the north slope model. The estimation by the north slope model of faster sap velocities than the south slope model in the south slope microclimate is due in roughly equal measure to a lack of soil moisture constraint and a more vigorous response to VPD. The radiation exchange produces this result because it frees the north slope model from serious light limitation.

on differing slope aspects. We will consider the differences in each partial function Φ in turn.

VPD: The parameterizations indicate that north slope madrones are more sensitive to shifts in VPD than their south slope counterparts (Figure 9). Our intuition about why this is the case is based on two population-level differences that we did not assess in the field, but can presume are present to some degree. Firstly, because of the stark differences in light environment between the two slopes of the hill, we expect that the relative abundances of sun-adapted and shade-adapted leaves differ in the overall composition of the madrone canopies representing each slope's population, with the north slope presumed to have more shade-adapted leaves than the south slope. There is a substantial body of literature describing the physiological differences between sun-adapted and shade-adapted leaves (Boardman, 1977; Larcher, 1995), but because these differences are usually described in terms of carbon assimilation rather than water use, directly relating them to differences in transpiration dynamics between the two populations is challenging. To do this we would need information about relative water use efficiencies, which leads to the second likely difference between the populations: differing canopy architectures along the lines of what is typical of sun-rich vs. shade-rich populations likely lead to differing light exposure regimes between the two populations. If, for instance, the proportion of leaf area accessing direct sunlight as opposed to indirect light, or even sunflecks, is less on the north slope, the north slope transpiration dynamics could be expected to be based on lower water use efficiencies, due to differing strategies of stomatal regulation (A. Knapp & Smith, 1987; Young & Smith, 1979). Woody vegetation using sunflecks as a light source have been shown to leave stomata open during moments of low light in order to assimilate the most carbon when leaves are illuminated (Stokes et al., 2010; Pearcy, 1998; A. K. Knapp & Smith, 1990). Thus, such differences in canopy architecture could result in tighter coupling between sap velocity and VPD in north slope canopies, due to the likely prevalence of exposed stomata on leaves that do not continuously experience the top-of-canopy sunlight dynamics. While the impact of differing proportions of sun-adapted vs shade-adapted leaves is obscured by an inability to resolve the exact mechanisms involved, we do suspect that this also plays a role in shaping the differences we observe. We thus speculate that, due to both lower light levels and disrupted exposure to what light there is, north slope trees are comparatively profligate wa-

ter users even in the midst of the dry summer, preferring to maximize carbon assimilation rather than conserve water.

Soil Moisture: The parameterizations indicate that north slope madrones are not water limited over the dry season. In our model, artificially increasing soil moisture for the north slope (i.e., 'watering' the trees) does not lead to increased sap velocity (see Figure 13, panel h). Nor does artificially increasing the soil moisture availability in the data feeding into the MCMC algorithm alter the resulting north slope parameters in meaningful ways (Figure 8). We hypothesize that this is because there is greater plant-available moisture on the north slope. The north slope has a deep water table (20 m) and a thick layer of weathered bedrock, and it has been shown to store around 30% of subsurface moisture in the vadose zone (Rempe & Dietrich, 2018; Vrettas & Fung, 2017). While there is evidence that trees on both slopes use this deep 'rock moisture' in the vadose zone for part of the dry season (Oshun, 2016), we have less data about the subsurface structure on the south slope, and data on respective rooting depths between the two populations is inconclusive (Oshun, 2016). However, the stronger sunlight on the south slope leads to higher evaporation, and the sap velocity data shows that the south slope trees cumulatively extract more water. Even if the subsurface structures and rooting depths were similar, there would be differences in water availability due to different rates of evaporation and vegetation extraction. Also, the north slope madrones grow in closer proximity to Douglas firs, which are known to exhibit hydraulic redistribution (Brooks et al., 2002, 2006), although we have no direct observations of this at our site. This could be further contributing to increased moisture availability in the north slope rooting zone.

Insolation: The parameterizations indicate that south slope madrones have a slightly greater overall sensitivity to insolation, and their overall insolation response function is shifted upwards from the north slope function (cf. Figure 9 panel c). The slightly higher sensitivity in the insolation response on the south slope could be explained by factors similar to those influencing VPD response, namely a higher fraction of leaves exposed to direct light, leading to stomatal regulation strategies that are more in phase with changes in light than those on the north slope. The upwards shift in the magnitude of the response could be explained by higher proportions of sun-adapted leaves in the south slope trees, which, due to their enhanced stomatal area (Boardman, 1977), could have higher rates of water use at every level of light intensity. In sum, we interpret that the north slope trees appear to have a larger area of stomata exposed under certain combinations of con-

ditions (lower light, higher VPD) while the south slope trees appear to have a larger area of stomata exposed under different combinations of conditions (higher light, and lower VPD).

3.7 Examination of residuals & limitations of analysis

Because the month of October stands out as a period of systematic error in figures 10 and 11, we focus first on the model errors in October, and then consider the remainder of the season separately. Firstly, the representation in a rough terrain of sunlight on the slopes scaled from a flat meadow observation becomes less accurate as the solar arc becomes lower in the sky (i.e., closer to the winter solstice), as shading from neighboring hills, especially in early morning and late afternoon, is site-specific. In particular, we are aware that the hill-shading received by our meadow-based light sensor begins substantially earlier in the day, in the late dry season, than the shading experienced by the trees under observation, which are positioned at a higher altitude. Secondly, we note that October began with a rain storm which was the only substantive moisture input during the period under observation. This rain event likely altered the relationship between surface and deep moisture reserves compared to the rest of the dry season, confounding the representativeness of our θ data stream for the month of October.

Apart from the month of October, the errors seem randomly distributed. We looked for, but did not find, correlations with wind speeds both in the time series and integrated over days. However, we can identify loose correlations of the residuals with daily integrated VPD. This suggests that there is a slight bias in our model towards overestimating sap velocity on exceptionally dry days, and underestimating it on more humid days.

Additionally, the model does not include variations of leaf area index through the summer. Madrones are evergreen, with leaf lifetimes of approximately 14 months, so that there are both old and new leaves between May and July (Ackerly, 2004). Studies have shown that the old leaves often contain less nitrogen than the new leaves on Pacific madrone (Adams, 1999), and it is thus reasonable to suppose that there are likely physiological differences in photosynthetic capacity, water use efficiency, or both between young and old leaves (e.g., as seen in Field et al. (1983)), which could be producing an effect not accounted for by our model expression.

Lastly, we acknowledge that our field site is small and the microclimates represented may not represent the extent of microclimatic variation across all north- and south-facing slopes in the broader ecosystem.

4 Conclusions

It is known that different species of vegetation exhibit a wide range of responses to ambient environment, which is pertinent knowledge to capturing several land-atmosphere biogeochemical cycles. However, we show that even within a single species, substantial variation can exist in the functional role that species plays in these biogeochemical cycles, based on acclimation to inhabited microclimate. In particular, 1) There are substantive and quantifiable microclimate differences between slopes; 2) There are substantive sap velocity differences between tree populations inhabiting the north and south slopes, and these indicate substantive transpiration differences between slopes; 3) A sap velocity model parameterized only with ambient microclimatic conditions captures sap velocity for our site well; and 4) The parameter differences in our sap velocity model represent different responses to ambient environment, and imply functional differences in tree physiology, between the two populations. This is suggestive of acclimation to inhabited microclimate.

Our results strongly hint at acclimation in leaf and canopy structure and differing stomatal regulation strategies (as in Wang et al. (2020)) between the two populations of trees. We suggest that north slope trees, limited by sunlight rather than soil moisture, have developed their canopies and stomatal regulation strategies to optimize for light capture while spending water more profligately than their south slope counterparts. Through this optimization, the north slope may be presumed to have different rates of carbon fixation per area of leaf and unit water transpired. This has implications for understanding water and carbon fluxes from forests today, and also for anticipating population-level profiles of vulnerability to future conditions.

Climate change is expected to alter current regimes of temperature (increase, Romero-Lankao et al. (2014)), VPD (increase, Grossiord et al. (2020)), precipitation (slight increase, although with decreased water availability, Romero-Lankao et al. (2014); Zamuda et al. (2013)), and cloudiness (unknown direction of change, Zamuda et al. (2013)) over California. All three of these changes directly impact the environmental covariates in this

model. The model results suggest that the south slope trees become severely water limited by the end of the dry season, and thus further water limitation may either limit their growing season, or create conditions that limit their performance. In contrast, on the north slope, the trees do not appear to be water limited. However, it is unclear whether this makes them more resilient to a hotter or dryer future. In our interpretation of parameter differences, north slope trees likely rely on much higher rates of water usage in order to assimilate carbon. If water becomes a limiting resource in the north-slope microclimate in the future, and VPD levels continue to increase, these north slope trees may be closer to crisis, choosing between cavitation or carbon starvation, than the south slope trees would be under a more limited growing season (Wang et al., 2020; Grossiord et al., 2020).

More measurements could help elucidate specific mechanisms underlying the parameter differences we have found. Direct measurements of photosynthesis/gas exchange on the leaf level, or chemical analyses of leaf tissues including C:N ratios or isotopic composition, could help shed light on physiological differences in leaves between populations. These measurements were not practical in our study given our lack of canopy access, but more measurements on these trees, or parallel investigations in a greenhouse, could be useful as a future study.

Acknowledgments

This project is supported by the DOE Office of Science grants DE-SC0010857 and DE-SC0014080 and NSF Eel River Critical Zone Observatory (EAR-1331940). TEB is also supported by a DOE Office of Science Graduate Student Research Fellowship. Data is available at DOI:10.5281/zenodo.3996308. The LiDAR data were provided by the National Center for Airborne Laser Mapping (NCALM). We thank Bill Dietrich and Daniella Rempe for detailed discussions about geology and subsurface moisture at the site; Charlie Koven, Jennifer Johnson and Joe Berry for comments on our sap velocity model interpretations; Colin Bode and David Elvins for support with solar modeling; and Colin Bode, Peter Steel, Chris Wong, Wendy Baxter, Anthony Ambrose, Katelyn Yu, Cecily Tye, Lian Zhang, Stephanie Wuerth, Michael Diaz, Andrew Levy, and Sheila Newbery for fieldwork support. The authors declare no conflicts of interest.

References

Ackerly, D. (2004). Functional strategies of chaparral shrubs in relation to seasonal water deficit and disturbance. *Ecological Monographs*, *74*(1), 25–44.

Adams, A. (1999). Arbutus menziesii and soils of the puget trough, washington. In A. Adams & C. W. Hamilton (Eds.), *The decline of pacific madrone (arbutus menziesii pursh): Current theory and research directions. proceedings of the april 28, 1995 symposium held at the center for urban horticulture university of washington seattle, washington subsequent research papers* (p. 139). Seattle: Save Magnolia's Madrones, Center for Urban Horticulture, Ecosystems Database Development Research.

Amitrano, C., Arena, C., Rouphael, Y., De Pascale, S., & De Micco, V. (2019). Vapour pressure deficit: The hidden driver behind plant morphofunctional traits in controlled environments. *Annals of Applied Biology*, *175*(3), 313-325.

Betancourt, M. (2017). A conceptual introduction to hamiltonian monte carlo. *arXiv preprint arXiv:1701.02434*.

Boardman, N. K. (1977). Comparative photosynthesis of sun and shade plants. *Annual review of plant physiology*, *28*(1), 355–377.

Bolton, D. (1980). The computation of equivalent potential temperature. *Monthly weather review*, *108*(7), 1046–1053.

Brooks, J. R., Meinzer, F. C., Coulombe, R., & Gregg, J. (2002). Hydraulic redistribution of soil water during summer drought in two contrasting pacific northwest coniferous forests. *Tree physiology*, *22*(15-16), 1107–1117.

Brooks, J. R., Meinzer, F. C., Warren, J. M., Domec, J.-C., & Coulombe, R. (2006). Hydraulic redistribution in a douglas-fir forest: lessons from system manipulations. *Plant, Cell & Environment*, *29*(1), 138–150.

Davis, T. W., Kuo, C.-M., Liang, X., & Yu, P.-S. (2012). Sap flow sensors: construction, quality control and comparison. *Sensors*, *12*(1), 954–971.

Duffie, J. A., & Beckman, W. A. (1991). *Solar engineering of thermal processes john wiley & sons*. John Willey & Sons.

Feddes, R., Kowalik, P., & Zaradny, H. (1978). *Simulation of field water use and crop yield john wiley and sons*. New York, NY: John Wiley and Sons.

Field, C., Merino, J., & Mooney, H. (1983). Compromises between water-use efficiency and nitrogen-use efficiency in five species of california evergreens. *Oe-*

cologia, *60*(3), 384–389.

Gimenez, B. O., Jardine, K. J., Higuchi, N., Negrón-Juárez, R. I., Sampaio-Filho, I. d. J., Cobello, L. O., ... Chambers, J. Q. (2019). Species-specific shifts in diurnal sap velocity dynamics and hysteretic behavior of ecophysiological variables during the 2015–2016 el niño event in the amazon forest. *Frontiers in Plant Science*, *10*, 830. Retrieved from `https://www.frontiersin.org/article/10.3389/fpls.2019.00830` doi: 10.3389/fpls.2019.00830

Gorelick, N., Hancher, M., Dixon, M., Ilyushchenko, S., Thau, D., & Moore, R. (2017). Google earth engine: Planetary-scale geospatial analysis for everyone. *Remote Sensing of Environment*. Retrieved from `https://doi.org/10.1016/j.rse.2017.06.031` doi: 10.1016/j.rse.2017.06.031

Granier, A. (1985). Une nouvelle méthode pour la mesure du flux de sève brute dans le tronc des arbres. In *Annales des sciences forestières* (Vol. 42, pp. 193–200).

Granier, A. (1987). Evaluation of transpiration in a douglas-fir stand by means of sap flow measurements. *Tree physiology*, *3*(4), 309–320.

Grossiord, C., Buckley, T. N., Cernusak, L. A., Novick, K. A., Poulter, B., Siegwolf, R. T. W., ... McDowell, N. G. (2020). Plant responses to rising vapor pressure deficit. *New Phytologist*, *226*(6), 1550–1566.

Harrison, J. L., Reinmann, A. B., Maloney, A. S., Phillips, N., Juice, S. M., Webster, A. J., & Templer, P. H. (2020). Transpiration of dominant tree species varies in response to projected changes in climate: Implications for composition and water balance of temperate forest ecosystems. *Ecosystems*, 1–16.

Hoffman, M. D., & Gelman, A. (2014). The no-u-turn sampler: adaptively setting path lengths in hamiltonian monte carlo. *Journal of Machine Learning Research*, *15*(1), 1593–1623.

Jarvis, P. G. (1976). The interpretation of the variations in leaf water potential and stomatal conductance found in canopies in the field. *Philosophical Transactions of the Royal Society of London. Series B, Biological Sciences*, *273*(927), 593–610. Retrieved from `http://www.jstor.org/stable/2417554`

Jasechko, S., Sharp, Z. D., Gibson, J. J., Birks, S. J., Yi, Y., & Fawcett, P. J. (2013). Terrestrial water fluxes dominated by transpiration. *Nature*, *496*(7445), 347–350.

Knapp, A., & Smith, W. (1987). Stomatal and photosynthetic responses during

sun/shade transitions in subalpine plants: influence on water use efficiency. *Oecologia*, *74*(1), 62–67.

Knapp, A. K., & Smith, W. K. (1990). Stomatal and photosynthetic responses to variable sunlight. *Physiologia Plantarum*, *78*(1), 160–165.

Larcher, W. (1995). *Physiological plant ecology, 3rd edition.* Springer-Verlag.

Lee, J.-H., Biging, G. S., & Fisher, J. B. (2016). An individual tree-based automated registration of aerial images to lidar data in a forested area. *Photogrammetric Engineering Remote Sensing*, *82*(9).

Link, P., Simonin, K., Maness, H., Oshun, J., Dawson, T., & Fung, I. (2014). Species differences in the seasonality of evergreen tree transpiration in a mediterranean climate: Analysis of multiyear, half-hourly sap flow observations. *Water Resources Research*, *50*(3), 1869–1894.

Link, P. A. (2015). *Forests, water, and the atmosphere in northern california: Insights from sap-flow data analysis and numerical atmospheric model simulations* (Unpublished doctoral dissertation). UC Berkeley.

Lohammar, T., Larsson, S., Linder, S., & Falk, S. O. (1980). Fast: Simulation models of gaseous exchange in scots pine. *Ecological Bulletins*(32), 505–523. Retrieved from `http://www.jstor.org/stable/20112831`

Mencuccini, M., Manzoni, S., & Christoffersen, B. (2019). Modelling water fluxes in plants: from tissues to biosphere. *New Phytologist*, *222*(3), 1207–1222.

Oliveras, I., & Llorens, P. (2001). Medium-term sap flux monitoring in a scots pine stand: analysis of the operability of the heat dissipation method for hydrological purposes. *Tree Physiology*, *21*(7), 473–480.

Oshun, J. (2016). *The isotopic evolution of a raindrop through the critical zone* (Unpublished doctoral dissertation). UC Berkeley.

Oshun, J., Dietrich, W. E., Dawson, T. E., & Fung, I. (2016). Dynamic, structured heterogeneity of water isotopes inside hillslopes. *Water Resources Research*, *52*(1), 164–189.

Pearcy, R. W. (1998). Acclimation to sun and shade. In A. S. Raghavendra (Ed.), *Photosynthesis: A comprehensive treatise* (p. 250-263). Cambridge: Cambridge University Press.

Rempe, D. M., & Dietrich, W. E. (2018). Direct observations of rock moisture, a hidden component of the hydrologic cycle. *Proceedings of the National*

Academy of Sciences, *115*(11), 2664–2669.

Romero-Lankao, P., Smith, J., Davidson, D., Diffenbaugh, N., Kinney, P., Kirshen, P., ... Villers Ruiz, L. (2014). North america. In C. F. D. D. M. M. K. M. T. B. M. C. K. E. Y. E. R. G. B. G. E. K. A. L. S. M. P. M. Barros V.R. & L.L.White (Eds.), *Climate change 2014: Impacts, adaptation, and vulnerability. part b: Regional aspects.* (p. 1439-1498). Cambridge, United Kingdom and New York, NY, USA: Cambridge University Press.

Salvatier, J., Wiecki, T. V., & Fonnesbeck, C. (2016). Probabilistic programming in python using pymc3. *PeerJ Computer Science*, *2*, e55.

Stafford, B. (2018, September). *pysolar.* Zenodo. Retrieved from `https://doi.org/10.5281/zenodo.1461066` doi: 10.5281/zenodo.1461066

Stokes, V. J., Morecroft, M. D., & Morison, J. I. (2010). Comparison of leaf water use efficiency of oak and sycamore in the canopy over two growing seasons. *Trees*, *24*(2), 297–306.

Sun, H., Aubrey, D. P., & Teskey, R. O. (2012). A simple calibration improved the accuracy of the thermal dissipation technique for sap flow measurements in juvenile trees of six species. *Trees*, *26*(2), 631–640.

USDA. (2008). *CALVEG zones and alliances: vegetation descriptions* (Tech. Rep.). Retrieved from `http://www.fs.usda.gov/Internet/FSE_DOCUMENTS/fsbdev3_046448.pdf`

Vrettas, M. D., & Fung, I. Y. (2017). Sensitivity of transpiration to subsurface properties: Exploration with a 1-d model. *Journal of Advances in Modeling Earth Systems*, *9*(2), 1030–1045.

Wang, Y., Sperry, J. S., Anderegg, W. R., Venturas, M. D., & Trugman, A. T. (2020). A theoretical and empirical assessment of stomatal optimization modeling. *New Phytologist*.

Ward, E. J., Domec, J.-C., King, J., Sun, G., McNulty, S., & Noormets, A. (2017). Tracc: an open source software for processing sap flux data from thermal dissipation probes. *Trees*, *31*(5), 1737–1742.

Waring, R. H., & Landsberg, J. J. (2011, 03). Generalizing plant–water relations to landscapes. *Journal of Plant Ecology*, *4*(1-2), 101-113. Retrieved from `https://doi.org/10.1093/jpe/rtq041` doi: 10.1093/jpe/rtq041

Young, D., & Smith, W. (1979). Influence of sunflecks on the temperature and water

relations of two subalpine understory congeners. *Oecologia*, *43*(2), 195–205.

Zamuda, C., Mignone, B., Bilello, D., Hallett, K., Lee, C., Macknick, J., ... Steinberg, D. (2013). *Us energy sector vulnerabilities to climate change and extreme weather* (Tech. Rep.). Department of Energy Washington DC.

Zhang, Q., Manzoni, S., Katul, G., Porporato, A., & Yang, D. (2014). The hysteretic evapotranspiration—vapor pressure deficit relation. *Journal of Geophysical Research: Biogeosciences*, *119*(2), 125-140. Retrieved from `https://agupubs.onlinelibrary.wiley.com/doi/abs/10.1002/2013JG002484` doi: 10.1002/2013JG002484